ANNUAL REVIEWS

*Annual Review of Earth and Planetary Sciences*

# A Holistic View of Climate Sensitivity

Nadir Jeevanjee, David J. Paynter, John P. Dunne, Lori T. Sentman, and John P. Krasting

NOAA/Geophysical Fluid Dynamics Laboratory, Princeton, New Jersey, USA; email: nadir.jeevanjee@noaa.gov

Annu. Rev. Earth Planet. Sci. 2025. 53:367–96

First published as a Review in Advance on February 19, 2025

The *Annual Review of Earth and Planetary Sciences* is online at earth.annualreviews.org

https://doi.org/10.1146/annurev-earth-040523-014302



## Keywords

climate sensitivity, climate modeling, forcing, feedback

## Abstract

The notion of climate sensitivity has become synonymous with equilibrium climate sensitivity (ECS), or the equilibrium response of the Earth system to a doubling of $CO_2$. But there is a hierarchy of measures of climate sensitivity, which can be arranged in order of increasing complexity and societal relevance and which mirror the historical development of climate modeling. Elements of this hierarchy include the well-known ECS and transient climate response and the lesser-known transient climate response to cumulative emissions and zero emissions commitment. This article describes this hierarchy of climate sensitivities and associated modeling approaches. Key concepts reviewed along the way include climate forcing and feedback, ocean heat uptake, and the airborne fraction of cumulative emissions. We employ simplified theoretical models throughout to encapsulate well-understood aspects of these quantities and to highlight gaps in our understanding and areas for future progress.

- There is a hierarchy of measures of climate sensitivity, which exhibit a range of complexity and societal relevance.
- Equilibrium climate sensitivity is only one of these measures, and our understanding of it may have reached a plateau.
- The more complex measures introduce new quantities, such as ocean heat uptake coefficient and airborne fraction, which deserve increased attention.

## 1. INTRODUCTION

Climate sensitivity is a primary raison d'etre of modern climate science, quantifying how global mean surface temperature responds to changes in carbon dioxide. Because many climate impacts scale with mean surface temperature [e.g., extreme temperature and precipitation (Seneviratne et al. 2016)], climate sensitivity encapsulates many aspects of the potential severity of global warming.

But formulating a precise definition of climate sensitivity raises difficult questions. Over what timescale should climate sensitivity be assessed? Should it be assessed in response to changes in $CO_2$ concentration, which is the variable most relevant for the greenhouse effect, or in response to $CO_2$ emissions, which is the quantity most directly influenced by human activity?

Climate science has responded by constructing several metrics of climate sensitivity, which are the subject of this review. We define them more precisely in Section 2, but briefly they are:

- Equilibrium climate sensitivity (ECS): The equilibrium temperature response to a doubling of atmospheric $CO_2$ concentrations.
- Transient climate response (TCR): The transient temperature response to a 1%/year increase in atmospheric $CO_2$, evaluated when the $CO_2$ concentration has doubled. The TCR includes the transient effects of ocean heat uptake and is smaller than ECS.
- Transient climate response to cumulative emissions (TCRE): The transient temperature response per unit of cumulative $CO_2$ emissions, usually quoted in Kelvin per gigatonne carbon (K/GtC). This metric accounts for transient carbon uptake by the land and ocean, as well as ocean heat uptake.
- Zero emissions commitment (ZEC): The change in temperature after emissions have been set to zero. ZEC is computed as the system approaches both thermal and chemical equilibrium, where the latter redistributes emitted carbon among the atmosphere, land, and ocean.

These metrics clearly span a spectrum of complexity, which also corresponds to their relevance. The TCRE and ZEC, which are the most complex metrics and account for the most processes, are also the most relevant and play a key role in international policy (Section 2.4). The metrics above are also interrelated, in that the more complex metrics are functions of the simpler ones (expressions in **Table 1**). A full understanding of climate sensitivity thus seems to require consideration of the entire hierarchy of metrics.

**Table 1 A hierarchy of climate sensitivities**

| Metric (acronym) | Model | $CO_2$ | OHFC(x) | SST(x) | Expression | Units |
|---|---|---|---|---|---|---|
| Cess sensitivity | AGCM | P | – | P | $\lambda[\Delta \mathrm{SST}(\mathbf{x})]$ | $\mathrm{W/m^2/K}$ |
| Equilibrium climate sensitivity (ECS) | SOM | P | P | I | $\frac{\mathcal{F}_{2\times}}{\lvert\lambda\rvert}$ | K |
| Transient climate response (TCR) | AOGCM | P | I | I | $\frac{\mathcal{F}_{2\times}}{\gamma+\lvert\lambda\rvert}$ | K |
| Transient climate response to cumulative emissions (TCRE) | ESM | I | I | I | $\frac{\alpha}{C_0}\mathrm{TCR}$ | K/GtC |
| Zero emissions commitment (ZEC) | ESM | I | I | I | $\frac{\alpha_\mathrm{f}/\alpha_\mathrm{ze}}{\mathrm{TCR/ECS}}-1$ (normalized) | K |

The various metrics of climate sensitivity along with their corresponding model configurations, with complexity increasing downward. As one descends the hierarchy, important boundary conditions such as SST, OHFC, and $CO_2$ concentration transition from being prescribed (P) to interactive (I), with model complexity increasing accordingly. Various analytical expressions for the sensitivities, developed in later sections, are also provided. Note that although ZEC has units of K, the expression for ZEC (from Equation 30) is normalized and hence dimensionless. Abbreviations: AGCM, atmosphere-only global climate model; AOGCM, atmosphere-ocean global climate model; ESM, Earth system model; OHFC, ocean heat flux convergence; SOM, slab-ocean model; SST, sea-surface temperature.

Historically, however, attention has not been distributed evenly across this hierarchy but has instead been focused on ECS (Charney et al. 1979, Mitchell et al. 1990, Knutti & Hegerl 2008). There are several reasons for this, including the simplicity of the definition of ECS, its encapsulation of both $CO_2$ radiative forcing and the all-important feedback parameter (Section 1.1), and the ability of ECS to capture intermodel spread in warming under realistic scenarios (e.g., Raper et al. 2002, Grose et al. 2018). This attention to ECS has paid off in a rather detailed understanding of forcing and feedback (Sherwood et al. 2020).

But we may have reached a point of strongly diminishing returns in our quest to understand ECS. The long, multi-millennial equilibration timescale of modern global climate models (GCMs) makes ECS nontrivial to evaluate (Dunne et al. 2020b, Rugenstein et al. 2020, Rugenstein & Armour 2021). Furthermore, the so-called pattern effect tells us that even if we could accurately evaluate ECS, the associated feedback parameter may not be relevant for near-term global warming (Section 3.5). Finally, ECS is unobservable in both a present-day and paleoclimate context, as fixing $CO_2$ concentrations for millennia is an unrealistic future scenario, and ECS does not account for certain Earth system feedbacks such as ice sheet and vegetation changes, which operate on longer timescales (Lunt et al. 2010, Previdi et al. 2013).

Given these limitations of ECS, our aim in this article is to zoom out and consider the full slate of sensitivity metrics outlined above as a coherent whole. The range of complexity of these metrics mirrors that of our climate models, and indeed each metric has coevolved with our modeling capabilities. We survey the role each metric plays in our understanding of climate change and take stock of how well we understand the metrics themselves. We take a theoretical approach throughout, highlighting where simple models capture Earth system behavior and where they do not, thus pointing out strengths and weaknesses in our understanding.

This article is thus not a review in the standard sense; we seek to be neither comprehensive in our coverage of topics nor exhaustive in our references to the literature. We do summarize important recent developments, and attempt to identify ways forward. We focus our attention on models [sometimes even just Geophysical Fluid Dynamics Laboratory (GFDL) models] to present our experience and point of view, but this in no way discounts the essential value of observations or other modeling approaches.

**GCM:** global climate model

**TOA:** top-of-atmosphere

**Longwave radiation:** thermal infrared radiation

**Shortwave radiation:** solar radiation, including visible and near-infrared frequencies

**OLR:** outgoing longwave radiation

**Albedo:** fraction of sunlight reflected

## 1.1. The Forcing-Feedback Framework

Before discussing the various metrics of climate sensitivity in more detail, we must set the stage with the forcing-feedback framework for global warming. In addition to Earth's global mean surface temperature[1] $T_s$, another key variable is Earth's top-of-atmosphere (TOA) net radiation balance,

$$N \equiv S - \mathrm{OLR} \qquad (\text{net radiation, W/m}^2), \qquad 1.$$

where $S$ is the net downward solar (or shortwave) radiation at the TOA, accounting for Earth's planetary albedo (fraction of sunlight reflected), and OLR is Earth's outgoing longwave radiation or thermal infrared radiation emitted to space at TOA. $N$ is positive when energy is accumulating in the system, and $N$ equals zero in equilibrium (although see sidebar titled Equilibrium Versus Steady-State in Climate Science).

[1]By surface temperature, we really mean near-surface air temperature, which can differ slightly from the land or ocean surface temperature (Cowtan et al. 2015). Also, in this article $T_s$ typically denotes a surface temperature anomaly from a climatological mean, although in a few cases (such as Equation 12) it denotes absolute temperature; such exceptions should be clear from context.

## EQUILIBRIUM VERSUS STEADY-STATE IN CLIMATE SCIENCE

In climate science, a state in which the TOA net radiation $N$ is equal to zero is conventionally referred to as thermal equilibrium. Thermodynamically speaking, however, this is a misnomer: $N = 0$ actually describes a *steady-state* balance between incoming radiation from the Sun and outgoing thermal radiation to space. Earth is not in equilibrium with either body, the net energy fluxes between them do not vanish, and Earth instead attains a temperature in between them. This should be contrasted with the behavior of the carbon cycle in Earth system models, in which $CO_2$ concentrations do truly equilibrate: There are no external sources or sinks of carbon, and the net carbon fluxes between the land, ocean, and atmosphere do vanish. Nonetheless, the use of the term equilibrium to describe a thermal steady-state in climate is ubiquitous, so we adopt this terminology here.

The forcing-feedback framework says that global warming can be divided into two processes that change $N$ in opposite ways. First, consider a change in atmospheric $CO_2$ (or any other radiatively active forcing agent) from an initial specific concentration $q_i$ to a perturbed concentration $q_f$, with all other variables (including $T_s$) held fixed. This induces a change in $N$, which is by definition the radiative forcing $\mathcal{F}$:

$$\mathcal{F} \equiv N(q_f) - N(q_i) \qquad (\mathrm{W/m^2}). \tag{2.}$$

The second process is that the surface temperature $T_s$ (and other climate variables) will respond to the forcing, causing countervailing changes in $N$ that eventually bring the system back to equilibrium ($N = 0$). This negative change in $N$ per unit $T_s$, which is typically dominated by increasing thermal emission to space (OLR) but may also include changes in $S$ due to albedo changes, is known as the feedback parameter:

$$\lambda \equiv \frac{dN}{dT_s} \quad (\mathrm{W/m^2/K},\ \lambda < 0). \tag{3.}$$

Together, these perturbations yield a net energy imbalance of

$$N = \mathcal{F} + \lambda T_s. \tag{4.}$$

This is the forcing-feedback decomposition of $N$.

Because $\lambda < 0$ in a stable climate, we often refer instead to the magnitude of the feedback parameter $|\lambda|$. The feedback parameter plays a key role, as a small value of $|\lambda|$ means that relatively large $T_s$ perturbations are required to significantly impact $N$, making the climate system more sensitive to perturbations as it tries to restore equilibrium.

## 2. A HIERARCHY OF CLIMATE SENSITIVITIES

We now survey the various metrics of climate sensitivity in greater detail, discussing how they are defined and computed and illustrating with simulations (**Figure 1**). As a guide, we organize these metrics vertically into a hierarchy in **Table 1**, with the most primitive measures of climate sensitivity at the top and more sophisticated measures that account for more processes toward the bottom. Accordingly, **Table 1** also includes a hierarchy of climate model configurations of varying complexity that exhibit a natural correspondence with the hierarchy of climate sensitivities. These model configurations are distinguished by whether important boundary conditions such as sea-surface temperature (SST), ocean heat flux convergence, and $CO_2$ concentration are externally prescribed or interactively simulated (predicted) by the model. This correspondence is discussed in more detail for each individual metric.

**SST:** sea-surface temperature

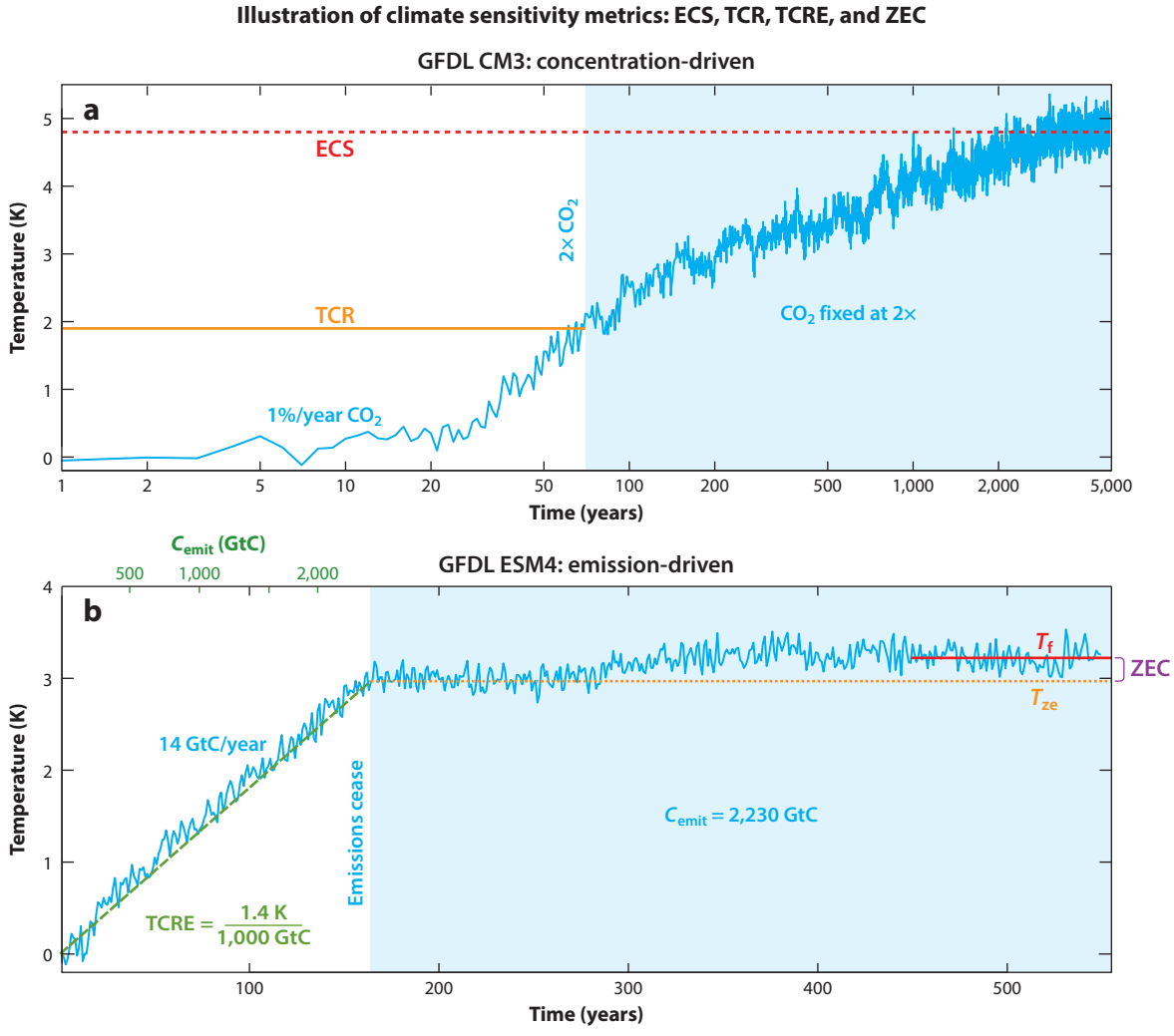


**Figure 1**

(*a*) Global mean surface temperature $T_s$ versus time for a multi-millennial atmosphere-ocean GCM simulation using GFDL CM3 (Donner et al. 2011, Paynter et al. 2018). $CO_2$ concentrations increase at 1%/year until doubling at year 70 and are held fixed thereafter. TCR is the warming at year 70, and ECS is the equilibrium warming after several millennia. Note the log time axis. (*b*) $T_s$ versus time for an Earth system simulation with an active carbon cycle using GFDL ESM4. Constant emissions of roughly 14 GtC/year are prescribed until roughly 3°C of warming, at which point emissions cease. The TCRE is the slope of $T_s$ versus cumulative emissions $C_{emit}$ (*green axis*, *upper left*) while emissions are nonzero, and ZEC is the difference between the final warming $T_f$ and the warming when emissions are zeroed $T_{ze}$. Abbreviations: ECS, equilibrium climate sensitivity; GFDL, Geophysical Fluid Dynamics Laboratory; GtC, gigatons carbon; TCR, transient climate response; TCRE, transient climate response to cumulative emissions; ZEC, zero emissions commitment.

## 2.1. Cess Sensitivity

**AGCM:** atmosphere-only GCM

Perhaps the most primitive notion of climate sensitivity is the Cess sensitivity, which is an estimate of λ obtained from atmosphere-only GCMs (AGCMs) operating over prescribed SSTs.[2]

[2]Land temperatures are determined interactively but largely follow the prescribed SSTs, e.g., **https://www.gfdl.noaa.gov/blog_held/11-is-continental-warming-a-slave-to-warming-of-the-ocean-surface/**.

**IPCC:** Intergovernmental Panel on Climate Change

Cess sensitivity is computed by running an AGCM simulation over a present-day or preindustrial SST distribution SST(**x**) and then running a second perturbation simulation over SST(**x**) + ΔSST, where ΔSST is typically a uniform perturbation of 2 or 4 K. The resulting TOA radiation perturbation $\Delta N$ divided by ΔSST yields an estimate of λ via Equation 3.

Because λ exerts a strong control on virtually every measure of climate sensitivity, including and especially ECS (Equation 6), it is of interest in model development to assess how λ differs between models and model versions. The Cess sensitivity has been useful in this regard in the past (Cess et al. 1989, Gettelman et al. 2012, Zhao et al. 2018).

However, the utility of the Cess sensitivity has diminished in recent years due to the pattern effect. As mentioned above and discussed further in Section 3.5, the pattern effect is the observation that λ does not take on a single well-defined value but instead depends on the spatial pattern of warming (Armour et al. 2013, Andrews et al. 2015, Gregory & Andrews 2016). In other words, if ΔSST(**x**) is a spatially varying SST perturbation due to global warming, then λ has a functional dependence on ΔSST(**x**), i.e.,

$$\lambda = \lambda[\Delta \mathrm{SST}(\mathbf{x})] \qquad \text{(pattern effect)}. \qquad 5.$$

Thus, while the Cess sensitivity remains a useful benchmark for comparing atmospheric models, it is unclear how a Cess sensitivity or λ calculated from a uniform SST increase might be related to the Cess sensitivity calculated from a more realistic warming pattern. There are also significant questions about what constitutes a realistic or relevant warming pattern, and on what timescale; this is discussed further in Section 3.5.

## 2.2. Equilibrium Climate Sensitivity

The next metric in **Table 1** is ECS, introduced in Section 1 as the equilibrium warming due to a doubling of $CO_2$ concentrations. ECS is conceptually the simplest sensitivity metric and has been a focus of climate science for decades. ECS was the subject of early calculations with 1D atmospheric models (Arrhenius 1896, Hulburt 1931, Callendar 1938, Plass 1956), culminating in the seminal work of Manabe & Wetherald (1967) who identified the necessary physical ingredients for a credible estimate of ECS (Jeevanjee et al. 2022). ECS has also been a mainstay of GCM intercomparisons and government assessment reports, beginning with the Charney report (Charney et al. 1979) and continuing on through many generations of assessments by the Intergovernmental Panel on Climate Change (IPCC) (e.g., Mitchell et al. 1990, Randall et al. 2007, Forster et al. 2021).

Throughout these reports, ECS has consistently been assessed at roughly 3°C, but with a relatively large likely range (66–100% probability) of roughly 1.5–4.5°C (Meehl et al. 2020). A major goal of climate science has been to reduce this uncertainty (Stevens et al. 2016), and recent years have in fact shown significant progress, with the likely range shrinking to roughly 2.6–4°C in the latest assessments (Sherwood et al. 2020, Forster et al. 2021).

A key ingredient in this achievement is the forcing-feedback framework of Section 1.1. Equilibrium requires that $N = 0$, i.e., that the increased radiation to space $|\lambda|T_s$ in Equation 4 balances the forcing $\mathcal{F}$. In the case of a doubling of $CO_2$, we write the forcing as $\mathcal{F}_{2\times}$ and Equation 4 then implies

$$\mathrm{ECS} = \frac{\mathcal{F}_{2\times}}{|\lambda|}. \qquad 6.$$

This forcing-feedback decomposition of ECS shows that ECS captures two of the most important determinants of climate change, $\mathcal{F}$ and λ, and conversely has allowed us to constrain ECS by constraining $\mathcal{F}$ and λ individually.

The calculation of ECS has a tortuous history. The first global calculations of ECS were performed in slab-ocean models (SOMs), or AGCMs coupled to shallow, motionless water columns that mimic the mixed layer of the real ocean and are thus able to interactively simulate SST(**x**) (Manabe & Stouffer 1980, Hansen et al. 1984). The horizontal transport of heat by ocean currents is represented by an externally prescribed ocean heat flux convergence OHFC(**x**) (units of $W/m^2$) (e.g., McFarlane et al. 1992). ECS can be straightforwardly computed in SOMs by doubling $CO_2$ and running the model to a new equilibrium, typically achieved within 30 years. As such, SOMs are a natural tool for calculating ECS, as suggested by **Table 1**. Indeed, even after the advent of fully coupled atmosphere-ocean GCMs (AOGCMs or coupled models) with a full-depth dynamical ocean, ECS was still calculated with SOMs (Meehl et al. 2005) because coupled models require millennia to equilibrate. This is illustrated in **Figure 1*a*** for GFDL's CM3 coupled model, which equilibrates after roughly 4,000 years.

In time, however, a practical workaround for calculating ECS from unequilibrated AOGCM simulations was developed by regressing TOA radiation imbalance $N$ against surface temperature $T_s$ and then extrapolating to equilibrium at $N = 0$ (Gregory et al. 2004, Danabasoglu & Gent 2009). This methodology became standard practice, using 150-year coupled simulations in which $CO_2$ was abruptly quadrupled and then held constant (abrupt4x simulations) (Taylor et al. 2012, Eyring et al. 2016).[3] But the pattern effect fundamentally complicates this method: The surface warming pattern and hence the feedback parameter can evolve with time (Section 3.5; **Figure 2**), so extrapolation is unreliable and tends to underestimate ECS (Dunne et al. 2020b, Rugenstein et al. 2020). Indeed, the ECS for CM3 found via a standard extrapolation method is 4°C (Andrews et al. 2012b), a roughly 20% underestimate of the model's true ECS of 4.8°C (**Figure 1*a***).

To resolve this tension, the regression-based ECS estimate has become known as the effective climate sensitivity, which is distinct from true, fully equilibrated ECS but can be viewed as a practical proxy for it (Rugenstein & Armour 2021). Indeed, the comprehensive assessment of Sherwood et al. (2020) is actually an assessment of effective climate sensitivity, not true ECS, allowing that work to leverage the widely performed and archived abrupt4x simulations. This approach has led to much progress and tighter constraints on ECS, as noted above and discussed further in Section 3. But the contortions required to study ECS in coupled models suggest there may be limits to this progress, and **Table 1** suggests that ECS is perhaps most naturally studied in SOMs. We comment further on this point in Section 7.

**SOM:** slab-ocean model

**Mixed layer:** the well-mixed upper layer of the ocean, typically 50–100 m in depth

**OHFC:** ocean heat flux convergence; the rate at which ocean currents converge heat into a column of ocean (in $W/m^2$)

**AOGCM:** coupled atmosphere-ocean GCM

**Abrupt4x:** coupled simulations in which $CO_2$ concentrations are abruptly quadrupled and then held fixed

**1pctCO2:** coupled simulations for probing transient climate change in which $CO_2$ concentrations are gradually increased at 1% per year

## 2.3. Transient Climate Response

The next rung in the climate sensitivity hierarchy is the TCR, a measure of the sensitivity of surface temperature to an increase in $CO_2$ concentrations over multi-decadal timescales, during which the interior ocean is far from equilibrium and hence so is $T_s$. Such transient warming was initially studied using 1D diffusive or upwelling-diffusion models of ocean heat uptake (e.g., Hoffert et al. 1980, Wigley & Schlesinger 1985). However, the precise definition of TCR was not formulated until the advent of transient AOGCM simulations in which it became conventional to gradually increase $CO_2$ concentrations by 1%/year (Washington & Meehl 1989, Manabe et al. 1991). TCR was then defined as the temperature anomaly averaged around year 70 of such a 1pctCO2 simulation, at which point $CO_2$ has doubled.[4]

[3]To improve the signal-to-noise ratio, $CO_2$ is often quadrupled rather than doubled, and the resulting temperature perturbation is divided by 2 to obtain ECS.

[4]This follows from the rule of 70, i.e., the time to doubling is $t = \frac{\ln 2}{\text{fractional growth rate}} \approx \frac{70}{\text{percentage growth rate}}$.

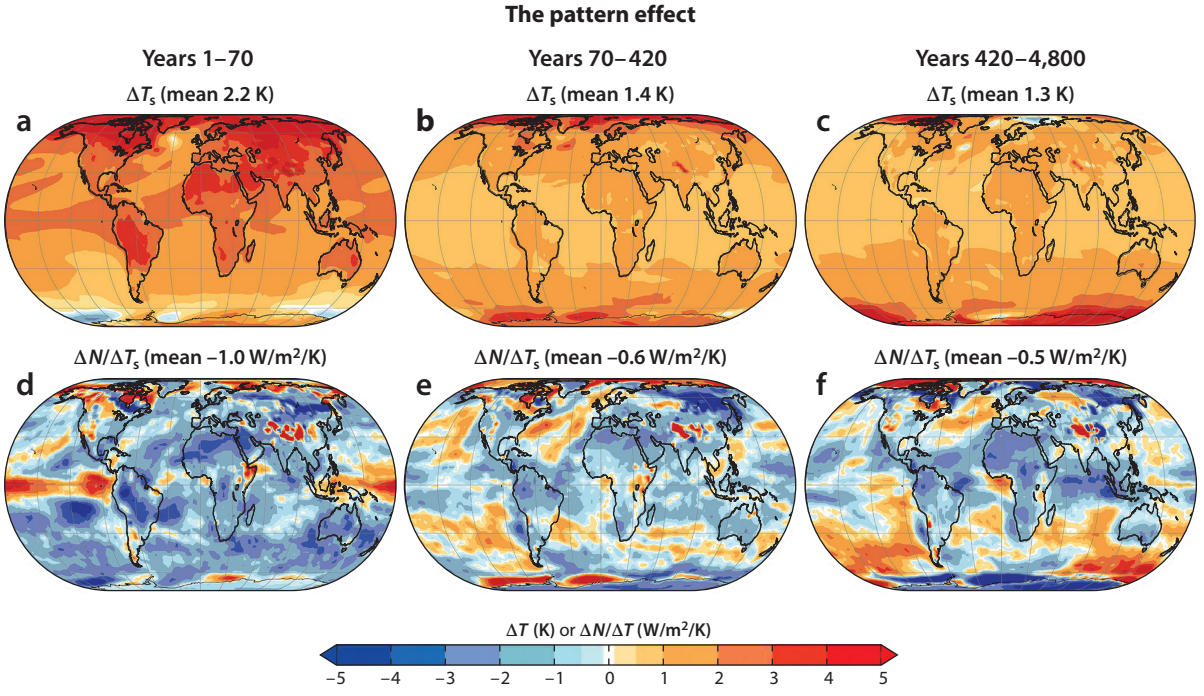


**Figure 2**

Maps of surface temperature change $\Delta T_s$ (*a–c*) and local feedback $\Delta N/\Delta T_s$ (*d–f*) for the CM3 simulation shown in **Figure 1*a***, where the changes are evaluated across the time periods specified at the top of each column. Global mean values for each field are in parentheses. Years 1–70 are the period of increasing $CO_2$, after which $CO_2$ is fixed at 2X preindustrial. The local feedback $\Delta N/\Delta T_s$ for a given period is calculated as local $\Delta N(\mathbf{x})$ divided by global mean $\Delta T_s$, and its global mean gives the corresponding feedback parameter $\lambda$. Between the first and last period, the spatial pattern of warming shifts dramatically, and the corresponding $\lambda$ changes by a factor of 2. Figure adapted from Paynter et al. (2018), figure 4.

The definition of TCR, and its relationship to ECS, is illustrated by the CM3 coupled model simulation shown in **Figure 1*a***, in which $CO_2$ concentrations are increased by 1%/year until year 70 and then held fixed for several millennia to allow for full equilibration. Such a scenario facilitates the calculation of TCR as well as true ECS from a single simulation. The TCR here is 1.9°C, close to the IPCC best estimate of 1.8 ± 0.4°C (likely range) (Forster et al. 2021).

As can be seen from the figure, in CM3 the TCR is slightly less than half of ECS, a typical result.[5] This is largely due to heat uptake by the deep subsurface ocean, which has an extremely large heat capacity, providing a significant heat sink for the surface mixed layer while it slowly equilibrates. These dynamics can be modeled rather simply with the two-box model of the ocean, discussed in Section 4. There it is argued that on the multi-decadal timescales relevant for TCR, the radiation imbalance is equal to the deep ocean heat uptake and can be written as

$$N = \gamma T_s, \qquad 7.$$

[5]The ratio of TCR to ECS, also known as the realized warming, does vary among models, however, and is an important indicator of the thermal disequilibrium between the surface and interior ocean (Stouffer & Manabe 1999, Raper et al. 2002).

where $\gamma$ is a constant known as the ocean heat uptake coefficient;[6] plugging this into Equation 4 and solving for $T_s$ yields an expression for TCR:

$$\mathrm{TCR} = \frac{\mathcal{F}_{2\times}}{\gamma + |\lambda|}. \quad 8.$$

**ESM:** Earth system model

Comparing Equation 8 to Equation 6 confirms that TCR < ECS due to ocean heat uptake. We discuss applications of Equation 8 in Section 4. It should be noted that heat uptake coefficient $\gamma$ has been much less studied than the feedback parameter $\lambda$; we comment further on this in Section 7.

## 2.4. Transient Climate Response to Cumulative Emissions and Zero Emissions Commitment

The final rungs in the climate sensitivity hierarchy of **Table 1** are the TCRE and ZEC. These quantities are defined in the context of Earth system model (ESM) simulations, which feature an interactive carbon cycle and hence explicitly simulate the exchange of carbon (and other biogeochemical quantities) between the land, atmosphere, and ocean. Because atmospheric $CO_2$ concentrations are typically interactive in ESMs rather than prescribed (**Table 1**), such models can then be used to simulate the climate response to $CO_2$ emissions rather than just the response to concentrations. Experiments with ESMs over the past 15 years or so have led to two striking findings that now form the basis for climate mitigation policy.

The first such finding is that global warming is proportional to cumulative emissions (e.g., Allen et al. 2009, Matthews et al. 2009, MacDougall 2016). This is illustrated in **Figure 1*b***, which shows an idealized simulation with GFDL's ESM4.1 (Dunne et al. 2020a) featuring constant emissions $E$ of roughly 14 GtC/year until 3°C of warming is reached, at which point emissions cease ($E = 0$). During the constant emissions phase the surface temperature $T_s$ increases roughly linearly with time $t$, and because the cumulative emissions $C_{\mathrm{emit}}(t) \equiv \int_0^t E(t')dt = Et$ are also linear in time (green axis in upper left of **Figure 1*b***), we indeed have

$$T_s \approx \Lambda C_{\mathrm{emit}}, \quad 9.$$

where the proportionality constant $\Lambda$ is by definition the TCRE. The TCRE for GFDL's ESM4 is $\Lambda \approx 1.4$ Kelvin per thousand gigatonnes carbon (K/1,000 GtC) (slope of green line in the left of **Figure 1*b***).

Like ECS and TCR, the precise value of TCRE is uncertain; it varies among models, with an IPCC best estimate of $1.65 \pm 0.65$°C (likely range) (Canadell et al. 2021). For a given model, however, the proportionality (Equation 9) is rather robust over time and across emissions scenarios, with a fixed value of $\Lambda$ (Matthews et al. 2009, Gillett et al. 2013, Herrington & Zickfeld 2014). The physics underlying this are reviewed in Section 6, but for the moment we emphasize that this robust proportionality of temperature to cumulative emissions has had major implications for policy. Most profoundly, it implies that net zero emissions are required to halt global warming: Because $E = dC_{\mathrm{emit}}/dt$, $E = 0$ is required to stabilize $T_s$.[7] Furthermore, Equation 9 implies that any temperature target (e.g., 1.5 or 2°C) should be associated with a cumulative emissions target, rather than a target $CO_2$ concentration or emissions rate (Allen et al. 2009, Matthews et al. 2012). This then implies a remaining carbon budget for a given temperature target, and indeed such a framework is now the norm for climate mitigation (Rogelj et al. 2019, Matthews et al. 2020). For

[6]This parameter is also often denoted with a $\kappa$ (Raper et al. 2002, Kuhlbrodt & Gregory 2012).

[7]It must be noted, however, that some climate impacts (such as sea level rise and ocean acidification) do not scale with $T_s$ and continue to increase even after emissions cease (e.g., Gillett et al. 2011).

## SYSTEM LINEARITY

A system responds linearly to forcing if its response to a sum of forcings equals the sum of the responses to the individual forcings. That is, if $X_i(t)$ is the response of a state variable $X$ to forcing $F_i(t)$, then linearity means that the response to $\sum_i F_i(t)$ is given by $\sum_i X_i(t)$. In this case, one may obtain the response to an arbitrary forcing by integrating that forcing against a Green's function (the response to a delta function forcing), as in Equation 11.

One explicit example of a linear system is the two-box model in Equation 17; in this case, system linearity manifests as the dependent variables occurring only linearly in the differential equations. Note that system linearity does not necessarily imply, nor is it implied by, a linear relationship between system variables. For further discussion in the context of climate sensitivity, see Gregory et al. (2015).

more on the connection between TCRE and the net zero paradigm for climate stabilization, see the comprehensive review of Allen et al. (2022).

The second remarkable and policy-relevant finding from ESMs, also apparent in **Figure 1*b***, is that temperatures roughly stabilize after $CO_2$ emissions cease. The change in temperature after emissions cease is defined to be the ZEC, and the finding is thus that

$$\mathrm{ZEC} \approx 0 \qquad 10.$$

(Matthews & Caldeira 2008, Solomon et al. 2009, MacDougall et al. 2020). We calculate ZEC for the simulation in **Figure 1*b*** as the difference between the final warming $T_\mathrm{f}$ (i.e., $T$ averaged over the past 100 years of the simulation) and the temperature at zero emissions $T_\mathrm{ze}$. This yields a ZEC for this scenario of roughly 0.2°C, which when normalized by $T_\mathrm{ze}$ is less than 0.1 and thus consistent with Equation 10.

Like the TCRE, ZEC varies across models but is typically small comparable to $T_\mathrm{ze}$ and quite close to zero when averaged across models, with an assessed value of ZEC $= 0 \pm 0.19$°C (likely range) (MacDougall et al. 2020, Canadell et al. 2021).[8] A near-zero ZEC is critical for the net zero and carbon budget paradigms, as a significantly nonzero ZEC would have to be accounted for in addition to $C_\mathrm{emit}$ in aiming to keep global warming below a given threshold (Rogelj et al. 2019). For a more detailed review of ZEC and its policy implications, see the review of Palazzo Corner et al. (2023).

What is the relationship between zero ZEC and constant TCRE? If surface temperature responds linearly to emissions (see the sidebar titled System Linearity), then these two phenomena are actually equivalent. To see this, we first note that Equation 10 holds for a variety of emissions profiles, including scenarios where an instantaneous pulse of carbon is emitted into the atmosphere (Matthews & Caldeira 2008, Matthews et al. 2009). We thus may approximate the temperature response to a unit emissions pulse as a step function $\Lambda\mathcal{H}(t)$, where $\mathcal{H}(t)$ is the unit step function. The response to an arbitrary emissions time series $E(t')$ can then be obtained by integrating $E(t')$ against this impulse response, i.e.,

$$T(t) = \int_0^t E(t')\Lambda\mathcal{H}(t-t')dt' = \Lambda\, C_\mathrm{emit}(t), \qquad 11.$$

reproducing Equation 9. The validity of this argument and the mechanisms behind ZEC and constant TCRE are discussed further in Section 6.

[8]This value of ZEC is assessed 50 years after emissions cease, for a scenario with final $C_\mathrm{emit}$= 1,000 GtC (MacDougall et al. 2020). For an analysis of ZEC on equilibrium timescales, see Tarshish et al. (2023). Also note that as in the IPCC AR6, we focus on the ZEC resulting from $CO_2$ forcing only; the behavior of ZEC in the presence of additional forcing agents can differ somewhat (Tarshish et al. 2023).

## 3. NEW PERSPECTIVES ON FORCING AND FEEDBACK

Having now surveyed the climate sensitivity hierarchy of **Table 1**, we spend the remainder of this article focusing on more specific topics related to each climate sensitivity measure. For Cess sensitivity and ECS, the key quantities are forcing and feedback, which we discuss in this section. Sherwood et al. (2020) provide a comprehensive review of those topics; here, we focus on a handful of recent developments, including in particular new analytical models for describing forcing and feedback in clear skies (Jeevanjee 2023, Koll et al. 2023, Stevens & Kluft 2023). We also discuss recent progress in assessing cloud feedbacks and the role these play in the pattern effect.

**IRF:** instantaneous radiative forcing, excludes rapid adjustments

**Rapid adjustment:** change in an element of the climate system, which impacts $N$ but is not due to changes in $T_s$

**ERF:** effective radiative forcing, includes rapid adjustments

### 3.1. Forcing

The concept of radiative forcing has evolved considerably over time (Ramaswamy et al. 2019). The radiative forcing described in Equation 2 is instantaneous radiative forcing (IRF), obtained as the change in $N$ when $CO_2$ (or other forcing agent; see the sidebar titled Non-$CO_2$ Forcing Agents) concentrations are changed and all other climate variables (surface and atmospheric temperatures, humidity, cloudiness, etc.) are held fixed. In the case of $CO_2$ forcing, it was found that the stratosphere cools in response to increased $CO_2$ (Manabe & Wetherald 1967, 1975), quickly and independently of any changes in $T_s$. This stratospheric adjustment then modifies the forcing felt by the tightly coupled surface-troposphere system (Houghton et al. 1994, Hansen et al. 1997). Subsequently it was understood that other elements of the climate system, especially clouds, also respond directly to changes in forcing agent concentrations independently of changes in $T_s$, and these other rapid adjustments also modify the forcing (Sherwood et al. 2015). This led to the concept of effective radiative forcing (ERF), which includes all these adjustments and is typically calculated by running fixed-SST AGCM experiments, changing the $CO_2$ (or other forcing agent) concentration, and calculating the corresponding change in $N$ (Hansen et al. 2005). For $CO_2$ the ERF is similar to the stratosphere-adjusted forcing, with a longtime estimate of roughly $\mathcal{F}_{2\times} \approx 4\,\mathrm{W/m^2}$ from benchmark calculations (Charney et al. 1979, Houghton et al. 1994, Sherwood et al. 2020).

In addition to longstanding confidence in the magnitude of $\mathcal{F}_{2\times}$, there has been recent progress in our understanding of $CO_2$ forcing, driven largely by a simple analytical model for clear-sky $CO_2$ IRF (Wilson & Gea-Banacloche 2012):

$$\mathcal{F} = 2l \ln\left(\frac{q_f}{q_i}\right)\left[\pi B(\nu_0, T_s) - \pi B(\nu_0, T_{\mathrm{strat}})\right]. \qquad 12.$$

Here $l = 10.2\,\mathrm{cm^{-1}}$ is a spectroscopic constant, $B$ is the Planck distribution in wavenumber space (wavenumber $\nu$ is defined as inverse wavelength, with unit $\mathrm{cm^{-1}}$), $\nu_0 = 667.5\ \mathrm{cm^{-1}}$ is the wavenumber at $CO_2$ band center, and $T_{\mathrm{strat}}$ is the emission temperature for wavenumbers near $\nu_0$, which emit from the stratosphere. For a pedagogical derivation and discussion of Equation 12, see Jeevanjee (2023). Note that Equation 12 applies only in the absence of water vapor but has been generalized to account for spectral overlap between $H_2O$ and $CO_2$ (Jeevanjee et al. 2021b).

Equation 12 has found several applications. Jeevanjee et al. (2021b) used it to explain the meridional gradient in $CO_2$ forcing. Seeley (2018) and later Romps et al. (2022) used it to establish the origin of the logarithmic scaling of $CO_2$ forcing, evident in the $\ln(q_f/q_i)$ factor in Equation 12. He et al. (2023) showed that the $T_s$ and $T_{\mathrm{strat}}$ dependence in Equation 12 implies a nonnegligible state dependence of $\mathcal{F}$, which also explains a significant amount of intermodel spread in $\mathcal{F}_{2\times}$. Wordsworth et al. (2024) deepened our understanding of Equation 12 by deriving the value of the spectroscopic constant $l$ from quantum-mechanical first principles.

As noted above, however, Equation 12 is only an expression for clear-sky $CO_2$ IRF. An extension to the all-sky case is clearly desirable, as is a deeper understanding of the stratospheric adjustment.

## NON-$CO_2$ FORCING AGENTS

Although $CO_2$ is the primary driver of present-day global warming, many other forcing agents contribute significantly to present-day and historical forcing. Most notable among these are other greenhouse gases such as methane, as well as aerosols such as sulfates, which provide a net negative forcing (Smith et al. 2020, Forster et al. 2021, Szopa et al. 2021).

The forcing-feedback framework assumes that all forcing agents give rise to the same global mean $T_s$ response per unit forcing. But given that some forcing agents such as aerosols are so short-lived that they are not well-mixed by the atmosphere, this is by no means obvious. This question has led to the notion of forcing efficacy, which measures the $T_s$ response to forcing from a given agent relative to that from an equal forcing from $CO_2$ (Hansen et al. 2005). Recent research suggests that models do on average exhibit forcing efficacies close to unity for most forcing agents, but for aerosols some models can exhibit nonunit efficacies (Richardson et al. 2019, Myhre et al. 2024).

Note that aerosol forcing consists of two components: the direct effect of scattering and absorption by the aerosols themselves and the indirect effect of aerosols on clouds as many aerosols serve as cloud condensation nuclei. In particular, the aerosol indirect effect is not well-understood, leading to uncertainties in present-day aerosol forcing that hamper efforts to constrain sensitivity metrics from present-day warming (Forster 2016, Bellouin et al. 2020).

The latter could lead to a model for $CO_2$ ERF, although other adjustments also exist, particularly cloud adjustments (Andrews et al. 2012a, Kamae et al. 2015).

### 3.2. The Planck Response and Its Drawbacks

We now turn to the feedback parameter $\lambda$. Again, Sherwood et al. (2020) provide a comprehensive resource, basing their approach on the conventional decomposition of $\lambda$ into the Planck response as well as water vapor, lapse rate, surface albedo, and cloud feedbacks, with detailed assessments of each (see also the comprehensive review of the water vapor and lapse rate feedbacks in Colman & Soden 2021). In this approach, the Planck response, defined as the change in $N$ due to a uniform warming of the surface and atmosphere while holding specific humidity fixed, is the reference response or null hypothesis for the climate response to warming, relative to which all other feedbacks are evaluated (Roe 2009). This conventional Planck feedback can be estimated by differentiating the Stefan–Boltzmann law with respect to a global average emission temperature $T_{em}$ satisfying OLR $= \sigma T_{em}^4$, yielding

$$\lambda_{reference} = \lambda_{planck} \approx -4\sigma T_{em}^3 \qquad 13.$$

(Cronin & Dutta 2023). But the assumption of fixed specific (rather than relative) humidity in the Planck response is unphysical and leads to spurious intermodel spread, correlations, and cancellations among the other feedbacks (Held & Shell 2012, Caldwell et al. 2016, Jeevanjee et al. 2021a). Assuming fixed relative humidity (RH) instead largely ameliorates these issues (Held & Shell 2012, Ingram 2013), but this fixed RH Planck response still assumes that high clouds warm in response to surface warming, contradicting the theoretically and observationally supported fixed anvil temperature hypothesis (discussed below). These drawbacks have motivated an emerging, complementary approach that focuses on the longwave clear-sky (LWCS) feedback (defined in the next section) rather than the Planck response as the basis for feedback analysis.

**Planck response:** change in $N$ due to uniform warming of surface and atmosphere

**LWCS:** longwave clear-sky

### 3.3. The Longwave Clear-Sky Feedback

Analogous to Equation 3, the LWCS feedback is defined as the negative change in clear-sky OLR with surface temperature:

$$\lambda_{\mathrm{LWCS}} \equiv -\frac{d\mathrm{OLR}_{\mathrm{cs}}}{dT_{\mathrm{s}}}. \qquad 14.$$

The clear-sky OLR is the OLR one would observe in the absence of clouds and can be computed in models as well as estimated from satellite observations, as referenced below.

By definition $\lambda_{\mathrm{LWCS}}$ excludes all effects from clouds but includes the effects from changes in water vapor and atmospheric temperature that conventionally have been encapsulated in the Planck, water vapor, and lapse rate feedbacks. Despite some uncertainty in these latter feedbacks, however, $\lambda_{\mathrm{LWCS}}$ itself is remarkably robust: Recent work has consistently found values of $\lambda_{\mathrm{LWCS}} \approx 2\ \mathrm{W/m^2/K}$, with an uncertainty of roughly 10% or so, across a hierarchy of models and observations (e.g., Koll & Cronin 2018, Zhang et al. 2020, Roemer et al. 2023). Such robustness suggests a relatively simple underlying mechanism, discussed below. That $\lambda_{\mathrm{LWCS}}$ is reasonably well-constrained and understood also makes it an apt starting point for feedback analyses, while also avoiding the drawbacks of the conventional Planck/lapse rate/water vapor decomposition.

The single-column model of Koll & Cronin (2018) suggested that $\lambda_{\mathrm{LWCS}}$ originates physically from the increase in surface radiation escaping to space through the transparent water vapor infrared window, consisting of wavenumbers between roughly 800 and 1,200 $\mathrm{cm^{-1}}$. The rest of the LW spectrum is dominated by atmospheric emission from $H_2O$, which turns out to be fairly insensitive to $T_s$, a fact sometimes referred to as Simpson's law (Ingram 2010, Koll & Cronin 2018, Jeevanjee et al. 2021a). Indeed, simply integrating the derivative of the Planck function across the water vapor window reproduces the expected value:

$$\lambda_{\mathrm{LWCS}} \approx -\int_{800\ \mathrm{cm^{-1}}}^{1200\ \mathrm{cm^{-1}}} \pi \frac{\partial B(\nu, T_{\mathrm{s}})}{\partial T_{\mathrm{s}}}\, d\nu \approx -2\ \mathrm{W/m^2/K} \qquad 15.$$

(Jeevanjee 2023, Stevens & Kluft 2023). Of course, this estimate is crude and more detailed analyses show that this surface feedback term makes up about two-thirds of $\lambda_{\mathrm{LWCS}}$, with the remainder emanating from the atmosphere (Feng et al. 2023, Koll et al. 2023). Nevertheless, Equation 15 remains a useful heuristic for understanding $\lambda_{\mathrm{LWCS}}$.

### 3.4. Cloud Feedbacks

In contrast to the robustness of the LWCS feedback, cloud feedbacks have long exhibited a large spread among GCMs, where even the sign of the net cloud feedback was long unknown (Zelinka et al. 2017). This has made cloud feedbacks an active area of research, and we highlight only a few salient points here. For thorough reviews, see Ceppi et al. (2017) and Sherwood et al. (2020) and the recent textbook by Siebesma et al. (2020).

Happily, recent years have seen a significant narrowing of the uncertainty in cloud feedbacks, due largely to the identification of large-scale cloud-controlling factors (such as local SST and atmospheric inversion strength) as independent variables for cloud radiative effects (Klein et al. 2017). Methodologies based on these variables have reduced uncertainty and increased confidence in a positive cloud feedback, driven largely by reduced shortwave reflection from marine low clouds (Zelinka et al. 2017, Ceppi & Nowack 2021, Myers et al. 2021).

Another significant cloud feedback stems from the high anvil clouds sitting atop thunderstorms, which tend toward higher altitudes with global warming so as to maintain a fixed cloud-top temperature, a fact known as the fixed anvil temperature or FAT hypothesis (Hartmann & Larson

**Water vapor window:** thermal infrared wavenumber range of roughly 800–1,200 $\mathrm{cm^{-1}}$ in which the atmosphere is largely transparent

**Cloud-controlling factors:** environmental variables determining cloud radiative effects

**FAT hypothesis:** fixed anvil temperature hypothesis, which says that the cloud-top temperature of high anvil clouds remains roughly constant under global warming

**Pattern effect:** dependence of feedback parameter λ on spatial pattern of SST change

2002, Thompson et al. 2017). This is interpreted in the conventional formalism as a positive feedback (even though the cloud-top longwave emission is unchanged), which is again an unphysical artifact of the Planck response (Yoshimori et al. 2020). This has motivated an alternative feedback decomposition in which the reference response is simply $\lambda_{LWCS}$, reduced by a factor that accounts for the masking of the clear-sky feedback by high clouds, whose thermal emission does not change and that cover a fraction $f_{high}$ of the domain:

$$\lambda_{reference} = (1 - f_{high})\lambda_{LWCS} \qquad 16.$$

(Jeevanjee 2023, Stevens & Kluft 2023, McKim et al. 2024).[9] Such a framework has yet to be fully explored but already has the advantage of encoding our current understanding in the reference response; any additional feedback terms then truly represent processes we do not understand well and that are worth isolating (Roe 2009).

## 3.5. The Pattern Effect

As mentioned in Sections 1 and 2.1, over the past decade the importance of the spatial pattern of SST changes on climate sensitivity has become apparent, in that λ has been found to depend rather significantly on the pattern of surface temperature change (Armour et al. 2013, Andrews et al. 2015, Gregory & Andrews 2016) (see also Equation 5).

This pattern effect is illustrated in **Figure 2**, which shows the spatial pattern of $\Delta T_s(\mathbf{x})$ and $\Delta N(\mathbf{x})$ (normalized by global mean $\Delta T_s$) over three different periods of the GFDL CM3 simulation from **Figure 1*a***. Over years 1–70, the warming is enhanced over land (relative to ocean) and over the Arctic relative to the rest of the globe, with suppressed warming over Antarctica and the Southern Ocean.[10] The later periods, and especially the last, show the Southern Hemisphere catching up, with warming now enhanced over Antarctica and the Southern Ocean. Most models also show enhanced warming over the Eastern Pacific relative to the west in later periods (Andrews et al. 2015), although this effect is not pronounced in CM3.

These variations in the SST pattern of warming give rise to cloud and other feedbacks that grow more positive over time, largely in the tropical Pacific and Southern Oceans (Ceppi & Gregory 2017). Indeed, a trend in Southern Ocean feedbacks can be seen in **Figure 2*d–f***. The impact on λ, which is simply the global mean of $\Delta N(\mathbf{x})/\Delta T_s$, can be quite significant; in **Figure 2**, λ varies by a factor of two between the first and last period. This shows that one must distinguish between the equilibrium feedback parameter $\lambda_{eq}$ that satisfies Equation 6 and a transient feedback parameter $\lambda_{tr}$ calculated in a transient scenario (Rugenstein & Armour 2021), such as the 1%/year period shown in **Figure 2*a*,*d***.[11]

A further complication due to the pattern effect is that historical AOGCM simulations are largely unable to match the observed pattern of warming, especially since 1980 or so (Wills et al. 2022). The disagreement in SST patterns is mostly in the Eastern Pacific and Southern Ocean, where as discussed above feedbacks (in particular cloud feedbacks) can vary significantly. Thus,

[9] In this framework, the impact of clouds on λ manifests as changes in cloud radiative effect, which are not the same things as cloud feedbacks (Soden et al. 2004) but have the advantage of being observable (Siebesma et al. 2020).

[10] These patterns are hallmarks of global warming and were predicted by our earliest climate models before they were observed, providing confidence in model projections (Manabe & Stouffer 1980, Manabe et al. 1991, Stouffer & Manabe 2017).

[11] This time dependence of the feedback parameter can equivalently be cast in terms of an ocean heat uptake efficacy, analogous to forcing efficacy where ocean heat uptake is thought of as a forcing on the ocean mixed layer as in **Figure 3** (see Winton et al. 2010, Geoffroy et al. 2013a, Rose & Rayborn 2016).

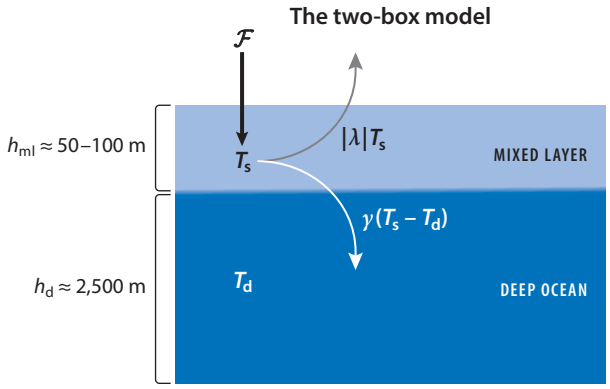


**Figure 3**

The ocean mixed layer responds to forcing $\mathcal{F}$ with a temperature anomaly $T_s$, which causes a change $|\lambda|T_s$ in net radiation to space as well as heat export to the deep ocean as $\gamma(T_s - T_d)$. Characteristic values for the mixed layer and deep ocean depths are $h_{ml} \approx 50–100$ m and $h_d \approx 2{,}500$ m, where the latter is the globally averaged ocean depth.

the real world can exhibit a historical feedback parameter $\lambda_{hist}$ that is different from both modeled $\lambda_{tr}$ and $\lambda_{eq}$, purely due to the pattern effect (Andrews et al. 2022, Armour et al. 2024). It is unclear whether the current $\lambda_{hist}$ is a product of internal variability and might gradually resemble modeled $\lambda_{tr}$ with time, or if instead the discrepancy between $\lambda_{hist}$ and modeled $\lambda_{tr}$ represents basic errors in the transient response of AOGCMs to radiative forcing. This question makes the pattern effect a major source of uncertainty in climate projections and an important problem for the field (Lee et al. 2022, Rugenstein et al. 2023, Watanabe et al. 2024).

## 4. MIXED-LAYER QUASI-EQUILIBRIUM AND THE TRANSIENT CLIMATE RESPONSE

Having surveyed forcing and feedback, the key ingredients of ECS (Equation 6), we now turn our attention to transient measures of climate sensitivity such as TCR and TCRE. In doing so we also shift our focus somewhat, from reviewing established frameworks and recent work to highlighting ideas and phenomena that call for greater exploration.

As noted in Section 2.3, ocean heat uptake plays a key role in transient climate change. A useful theoretical framework for ocean heat uptake and transient climate change is the two-box model (Held et al. 2010, Geoffroy et al. 2013b), which we introduce here. This model consists of a shallow, mixed-layer ocean of heat capacity $C_s$ (J/m$^2$/K) and temperature anomaly $T_s$ coupled to a much larger deep ocean with heat capacity $C_d \gg C_s$ and temperature anomaly $T_d$. The radiative forcing $\mathcal{F}$ and increased radiation to space $|\lambda|T_s$ are, respectively, absorbed and emanated by the mixed layer, which also exports energy to the deep ocean in linearized form as $\gamma(T_s - T_d)$. Here $\gamma$ is again the deep ocean heat uptake coefficient in W/m$^2$/K. This model is pictured in **Figure 3**, and the corresponding equations are

$$C_s \frac{dT_s}{dt} = \mathcal{F} - |\lambda|T_s - \gamma(T_s - T_d) \qquad 17a.$$

$$C_d \frac{dT_d}{dt} = \gamma(T_s - T_d). \qquad 17b.$$

**MLQE:** mixed-layer quasi-equilibrium, in which the forcing, net radiation to space, and deep ocean heat uptake all balance

A key property of these equations is that the response timescales of $T_s$ and $T_d$ differ markedly, due to the difference in $C_s$ and $C_d$ (which stems from the difference in globally averaged mixed layer and deep ocean depth, roughly $h_{ml} \approx 50-100$ m and $h_d \approx 2{,}500$ m). Indeed, a preliminary analysis shows that these timescales can be estimated as[12]

$$\tau_s = \frac{C_s}{\gamma + |\lambda|} \approx 3-6 \text{ years} \tag{18a.}$$

$$\tau_d = C_d \frac{\gamma + |\lambda|}{\gamma |\lambda|} \approx 700 \text{ years.} \tag{18b.}$$

If the system is driven by a forcing $\mathcal{F}(t)$ that is monotonic over timescales longer than $\tau_s$ and shorter than $\tau_d$ (i.e., multi-decadal), one can make the approximations $C_s = 0$ and $C_d = \infty$, which yield a mixed layer in quasi-equilibrium ($\frac{dT_s}{dt} = 0$) with a deep ocean that has not yet responded ($T_d = 0$). In such a mixed-layer quasi-equilibrium (MLQE), the ocean heat uptake is simply $\gamma T_s$ (as in Equation 7) and Equation 17a implies that the arrows going into and out of the mixed layer in **Figure 3** must balance, hence

$$T_s \approx \frac{\mathcal{F}}{\gamma + |\lambda|} \qquad \text{(MLQE).} \tag{19.}$$

This simple equation suggests that for transient scenarios in which $\mathcal{F}$ varies on multi-decadal timescales, temperature should be proportional to forcing (Gregory & Forster 2008). This should apply to historical warming as well as 1%/year scenarios and in particular should apply to the definition of TCR as the warming at year 70. Applying Equation 19 to this instance then yields the expression for TCR previously quoted in Equation 8:

$$\text{TCR} \approx \frac{\mathcal{F}_{2\times}}{\gamma + |\lambda|}. \tag{20.}$$

If we now combine Equations 19 and 20, we find that we can estimate transient warming in any scenario for which MLQE holds by scaling the TCR by the time-dependent forcing $\mathcal{F}(t)$:

$$T_s(t) \approx \frac{\mathcal{F}(t)}{\mathcal{F}_{2\times}} \text{TCR}. \tag{21.}$$

This scaling has been noted before (Gregory & Forster 2008) and utilized in observational estimates of ECS and TCR (e.g., Otto et al. 2013), but its general validity has not been fully examined or emphasized. Here, we illustrate both the proportionality (Equation 19) and the TCR scaling (Equation 21) for the GFDL CM4 coupled model (Held et al. 2019). **Figure 4** scatterplots annual mean, global mean $\mathcal{F}(t)$ against $T_s(t)$ for various scenarios, including historical runs extended to 2100 via the SSP2-4.5 scenario (O'Neill et al. 2016) with differing forcing agents, as well as for a 1pctCO2 scenario extended to 140 years to quadrupled $CO_2$. Forcing time series are ERF calculated from fixed-SST simulations (Section 3.1), whereas $T_s(t)$ is drawn from the usual coupled simulations. The straight line in **Figure 4** also shows the scaling (Equation 21), using GFDL CM4's characteristic values of $\mathcal{F}_{2\times} = 4$ W/m$^2$ and TCR = 2 K (Winton et al. 2020).

Almost all the simulation data in **Figure 4** collapse onto the same quasi-linear curve, including that from the HIS-AER simulation (aerosol only, green dots), which includes only negative

[12] For a derivation of Equation 18, see Jeevanjee (2023). To evaluate Equation 18, we set $C_s = \rho_w C_w h_{ml}$ and $C_d = \rho_w C_w h_d$, where $\rho_w = 1{,}024$ kg/m$^3$ and $C_w = 3{,}850$ J/kg/K are the density and specific heat of seawater, respectively. We also take typical values of $|\lambda| = 1.3$ W/m$^2$/K (Sherwood et al. 2020) and $\gamma = 0.7$ W/m$^2$/K (Geoffroy et al. 2013b).

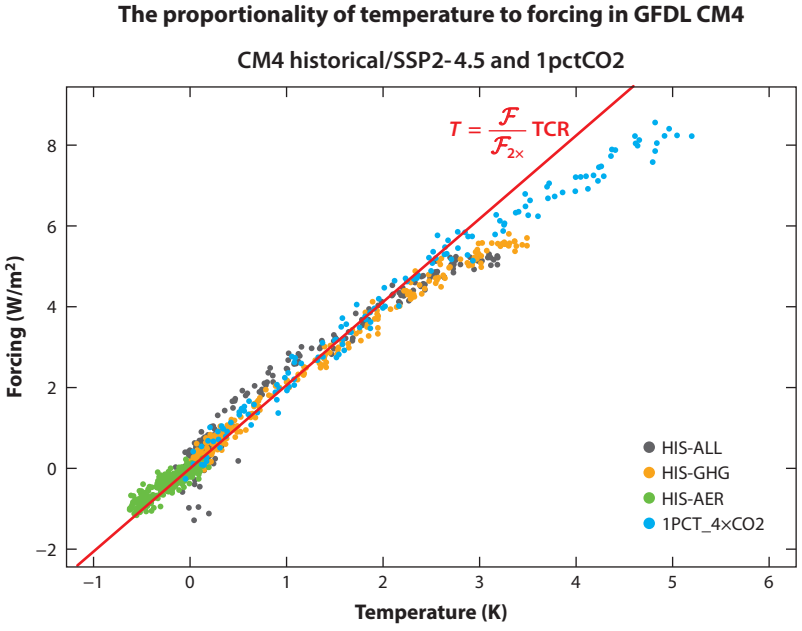


**Figure 4**

Testing the proportionality of temperature to forcing for GFDL CM4, for variants of the historical/SSP2-4.5 scenario as well as a 1pctCO2 scenario run to 4XCO2 (*colored* and *black dots*, annual and global means), along with the scaling (Equation 21) (*red line*). The HIS-ALL scenario includes all forcing agents (anthropogenic and natural), HIS-GHG includes only greenhouse gases, and HIS-AER includes only aerosol forcing. The scaling (Equation 21) provides a reasonable approximation to the simulated evolution over multi-decadal timescales, with some deviation at later times and larger amounts of warming. Abbreviation: GFDL, Geophysical Fluid Dynamics Laboratory.

forcing and temperature perturbations. Furthermore, the TCR scaling (Equation 21) provides a reasonable estimate of this curve, especially for forcings less than 5 W/m$^2$ or so. Beyond that the MLQE approximation breaks down, largely due to the pattern effect and nonnegligible warming of the deep ocean and its impacts on ocean heat uptake (Equation 22) (Gregory et al. 2015).[13] The scaling (Equation 21) thus suggests that for near-term transient warming, a projection of $\mathcal{F}(t)$ and knowledge of TCR are sufficient to project global warming, underscoring the utility of TCR.

## 5. ON THE CURVATURE OF OCEAN HEAT UPTAKE AND LIMITATIONS OF THE TWO-BOX MODEL

The last section highlighted the utility of the MLQE approximation and TCR in describing transient warming on multi-decadal timescales. But, the MLQE approximation (Equation 19) assumes $C_d = \infty$ and hence $T_d = 0$, assumptions that must break down over longer timescales. If we instead utilize the deep-layer version of the two-box model (Gregory et al. 2015) in which we keep $C_s = 0$ but now allow $C_d$ to be finite, so that the mixed layer is always in quasi-equilibrium but with a

[13] In the HIS-ALL case, one can also see a few black dots at low $T_s$ values that deviate from the linear scaling; these are precisely the years of large volcanic eruptions whose forcings dissipate on timescales shorter than $\tau_s$ and whose climate response is therefore not expected to obey the MLQE relation (Equation 19) (Gregory & Forster 2008).

deep ocean whose temperature $T_d$ is nonzero and evolving, Equation 17a then yields

$$T_s = \frac{\mathcal{F} + \gamma T_d}{|\lambda| + \gamma} \qquad \text{(deep-layer model)}. \tag{22.}$$

**OHC:** ocean heat content (Joules)

This implies that $T_s$ increases supralinearly with $\mathcal{F}$, contributing to the curvature in **Figure 4**. Indeed, Geoffroy et al. (2013b) accurately fit the full two-box model (Equation 17) to an ensemble of 150-year abrupt4x and 1pctCO2 simulations, largely capturing the curvature in $T_s$ versus $\mathcal{F}$ (or equivalently time) for the 1pctCO2 simulations. Thus, the full two-box model seems able to accurately capture the evolution of $T_d$ and hence ocean heat uptake in AOGCMs, at least on 150-year timescales.

But the validity of the two-box model on longer timescales remains relatively unexplored. The deep ocean timescales diagnosed by Geoffroy et al. (2013b) of roughly 250 years are short relative to the simple estimate of 700 years from Equation 18b, which may simply be a consequence of fitting to 150-year simulations. Here, we use much longer millennial abrupt4x simulations from LongRunMIP (Rugenstein et al. 2020) to further probe the ability of the two-box model to emulate deep ocean heat uptake.

We aim to compare the predictions of the deep-layer model with LongRunMIP abrupt4x output of $T_s$ and net TOA energy imbalance $N$. To that end, we note that in the deep-layer model,

$$N = \gamma(T_s - T_d) = C_d \frac{dT_d}{dt}, \tag{23.}$$

so the entire global energy imbalance resides in the deep ocean. Integrating Equation 23 over Earth's area and over time then yields two expressions for the total ocean heat content (OHC), in Joules:

$$\mathrm{OHC}(t) = A_{\mathrm{Earth}} \int_0^t N(t')dt' \tag{24a.}$$

$$= C_w M_{\mathrm{ocean}} T_d. \tag{24b.}$$

Here $A_{\mathrm{Earth}} = 5.1 \times 10^{14}\,\mathrm{m}^2$ is the area of Earth, $M_{\mathrm{ocean}} = 1.37 \times 10^{21}$ kg is the mass of the world ocean, and $C_w = 3{,}850\,\mathrm{J/kg/K}$ is the specific heat of seawater. Equation 24a allows us to calculate OHC from simulated $N$, whereas Equation 24b allows us to relate OHC to the two-box model. Note that in the two-box model under an abrupt4x scenario, the equilibrium values of both $T_s$ and $T_d$ are 2ECS, with a corresponding equilibrium OHC of $\mathrm{OHC}_{\mathrm{eq}} \equiv 2\,C_w M_{\mathrm{ocean}}\mathrm{ECS}$ (also see the sidebar titled Differences Between ECS and Interior Ocean Warming).

## DIFFERENCES BETWEEN ECS AND INTERIOR OCEAN WARMING

It is notable that for the fully equilibrated simulations in **Figure 5** (CESM1, GISSE2R, and MPI-ESM1.1), the equilibrated OHC is 10–25% less than the ECS-based estimate $\mathrm{OHC}_{\mathrm{eq}}$. Because ECS is evaluated using global mean near-surface air temperature, this discrepancy can be attributed to multiple drivers, including land warming more than ocean (Sutton et al. 2007) and oceanic near-surface air warming more than the underlying SSTs (Cowtan et al. 2015). Furthermore, abyssal ocean warming can be suppressed relative to SST warming even in equilibrium by continued deep water formation, which varies across models: Some models show fairly uniform equilibrium warming with depth (Li et al. 2013), while others exhibit significantly suppressed warming at depth, which can be modulated by varying ocean mixing parameters (Krasting et al. 2018).

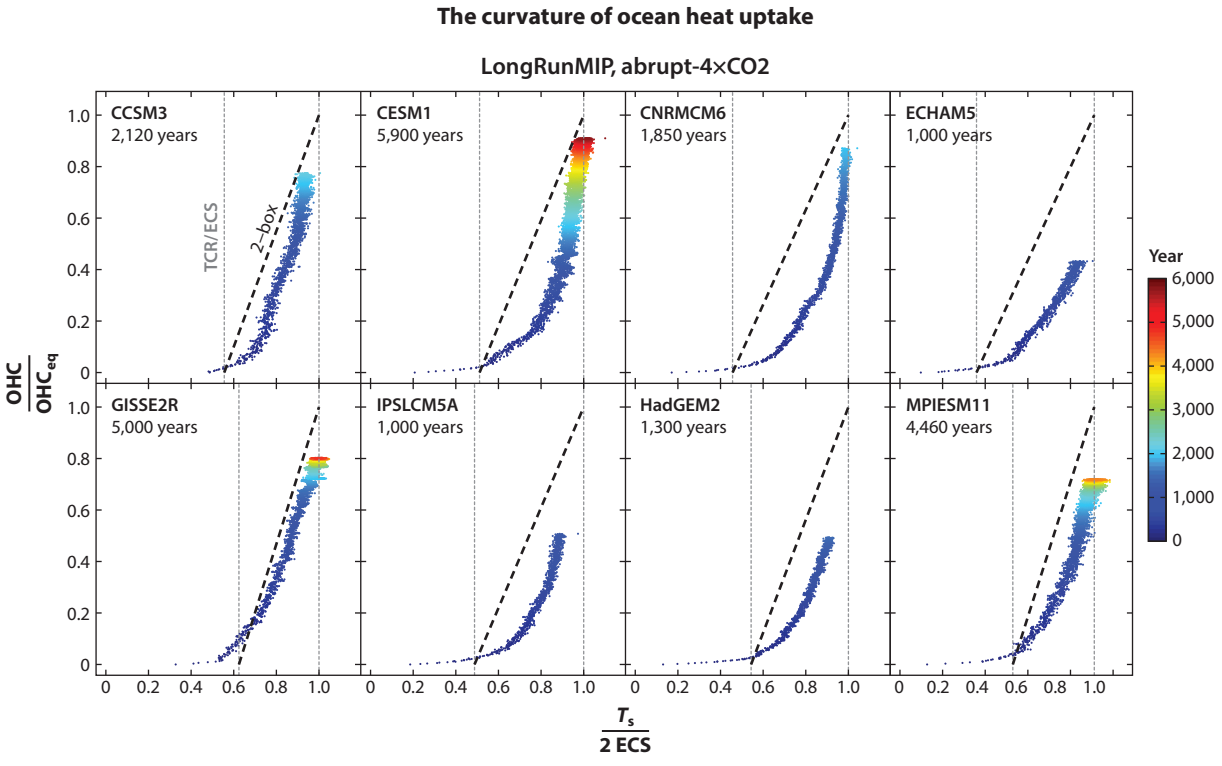


**Figure 5**

Normalized OHC versus normalized $T_s$ for LongRunMIP abrupt-4xCO2 simulations from various models (*colored dots*; colors indicate simulation year per the color bar in the *lower right*). Also shown is the straight line two-box model prediction (25) (*thick dashed line*), with $x$-intercept of TCR/ECS (*left-hand thin dashed line* in each panel). Many models display significant curvature in this measure of ocean heat uptake, in contrast to the straight line two-box prediction. Abbreviation: OHC, ocean heat content.

Normalizing $T_s$ and OHC by these equilibrium values, differentiating Equation 24b with respect to $T_s$, and invoking Equations 6, 8, and 22, one obtains after some manipulation

$$\frac{d(\mathrm{OHC}/\mathrm{OHC}_{eq})}{d(T_s/2\mathrm{ECS})} = \frac{dT_d}{dT_s} = \frac{1}{1-\frac{\mathrm{TCR}}{\mathrm{ECS}}}. \qquad 25.$$

Note that $dT_d/dT_s > 1$ because both $T_s$ and $T_d$ must approach the same value at equilibrium, but $T_s$ gets a head start in the first 5–10 years due to its rapid quasi-equilibration, so $T_d$ must subsequently warm faster than $T_s$.

**Figure 5** shows normalized OHC versus $T_s$ as simulated by various LongRunMIP models, where TCR and ECS values for each model are obtained from the literature (e.g., Meehl et al. 2020, Nijsse et al. 2020). For models with runs longer than 4,000 years, however, we take 2ECS as the average $T_s$ over the last 500 years of the run. Equation 25 predicts that normalized OHC versus $T_s$ is a straight line with slope 1/(1 − TCR/ECS), shown in the thick dashed line, with $x$-intercept of TCR/ECS (left-hand thin dashed line in each panel). While some models have an evolution similar to this straight line (e.g., CCSM3 and GISSE2R), it is evident that many models display significant curvature in their deep ocean heat uptake, including models whose slope of simulated OHC versus $T_s$ can be much steeper than the two-box prediction (e.g., CNRMCM6).

In such models, the deep ocean can warm with very little impact on $T_s$ (as also found in, e.g., Li et al. 2013, Krasting et al. 2018). It would be of interest to see if diffusive models (e.g., Harvey 2018) or the more elaborate model of Marshall & Zanna (2014) is better able to capture this phenomenon.[14] In either case, the diversity of this ocean heat uptake curvature among models and its general incongruence with the two-box model indicate that there is still much to learn about ocean heat uptake.

## 6. UNDERSTANDING TRANSIENT CLIMATE RESPONSE TO CUMULATIVE EMISSIONS AND ZERO EMISSIONS COMMITMENT

We now turn to the two final rungs of **Table 1** concerning the sensitivity of Earth's climate to $CO_2$ emissions rather than concentrations.

Recall from Section 2.4 that the TCRE is defined as the ratio of surface temperature change $T_s$ to cumulative emissions $C_{emit}$, and that constant TCRE actually follows from ZEC = 0 by Equation 11, assuming system linearity. **Figure 1*b*** showed that $T_s$ is indeed proportional to $C_{emit}$ in GFDL ESM4.1 for a given emissions scenario of $E = 14$ GtC/year; now we examine whether this holds true for additional emissions scenarios of 10 GtC/year and 1pctCO2. (In the latter simulation, emissions are adjusted online to ensure that $CO_2$ concentrations rise as prescribed.)

**Figure 6*a*** shows the emissions trajectories $C_{emit}(t)$. The corresponding temperature trajectories $T_s(t)$, shown in **Figure 6*c***, track the emissions trajectories quite closely. Accordingly, plotting $T_s$ versus $C_{emit}$ in **Figure 6*d*** then collapses the various scenarios onto a fairly straight line whose slope is the TCRE of roughly 1.4 K/(1,000 GtC) (cf. **Figure 1*b***).

Why does this collapse occur? From Equation 19 and **Figure 4**, we already expect a rough proportionality between temperature and forcing. How does this extend to a proportionality between temperature and (cumulative) emissions? The ratio of $CO_2$ concentrations appearing in the $CO_2$ forcing expression (Equation 12) can be related to cumulative emissions $C_{emit}$ as

$$\frac{q_f}{q_i} = \frac{C_0 + \alpha C_{emit}}{C_0}, \qquad 26.$$

where $C_0 = 590$ GtC is the preindustrial atmospheric $CO_2$ mass[15] and $\alpha$ is the airborne fraction, i.e., the fraction of $C_{emit}$ that still resides in the atmosphere at a given time. The airborne fraction is thus the key degree of freedom relating $C_{emit}$ and forcing, and hence it is a key parameter in determining TCRE. Indeed, if we calculate TCRE at the time of doubling in an ESM 1pctCO2 simulation (Gillett et al. 2013), then $T_s = \text{TCR}$ and $\alpha C_{emit} = C_0$ and we have

$$\Lambda = \frac{\alpha}{C_0}\text{TCR}. \qquad 27.$$

This formula, also recorded in **Table 1**, shows that TCRE is determined directly by $\alpha$ and TCR. Equation 27 was also used by the IPCC to estimate $\Lambda$: Indeed, invoking their central estimates of TCR = 1.8°C and $\alpha = 0.53$ yields a value almost identical to their previously quoted value of $\Lambda = 1.65$ K/(1,000 GtC) (Canadell et al. 2021).

Returning to the question of the collapse in **Figure 6*d***, we substitute Equation 26 into the forcing expression (Equation 12) and substitute that into the approximate TCR scaling

[14]Note that the pattern effect cannot account for this curvature, as Equation 25 shows that $|\lambda_{eq}| < |\lambda_{tr}|$ makes TCR/ECS smaller and hence the slope $dT_d/dT_s$ shallower, not steeper. On another note, it is worth remarking that diffusive models of ocean heat uptake also support the scaling (Equation 21); see **https://www.gfdl.noaa.gov/blog_held/51-the-simplest-diffusive-model-of-oceanic-heat-uptake-and-tcr/**.

[15]Obtainable as the preindustrial $CO_2$ concentration of 278 ppm multiplied by a standard conversion factor of 2.124 GtC/ppm (Friedlingstein et al. 2020).

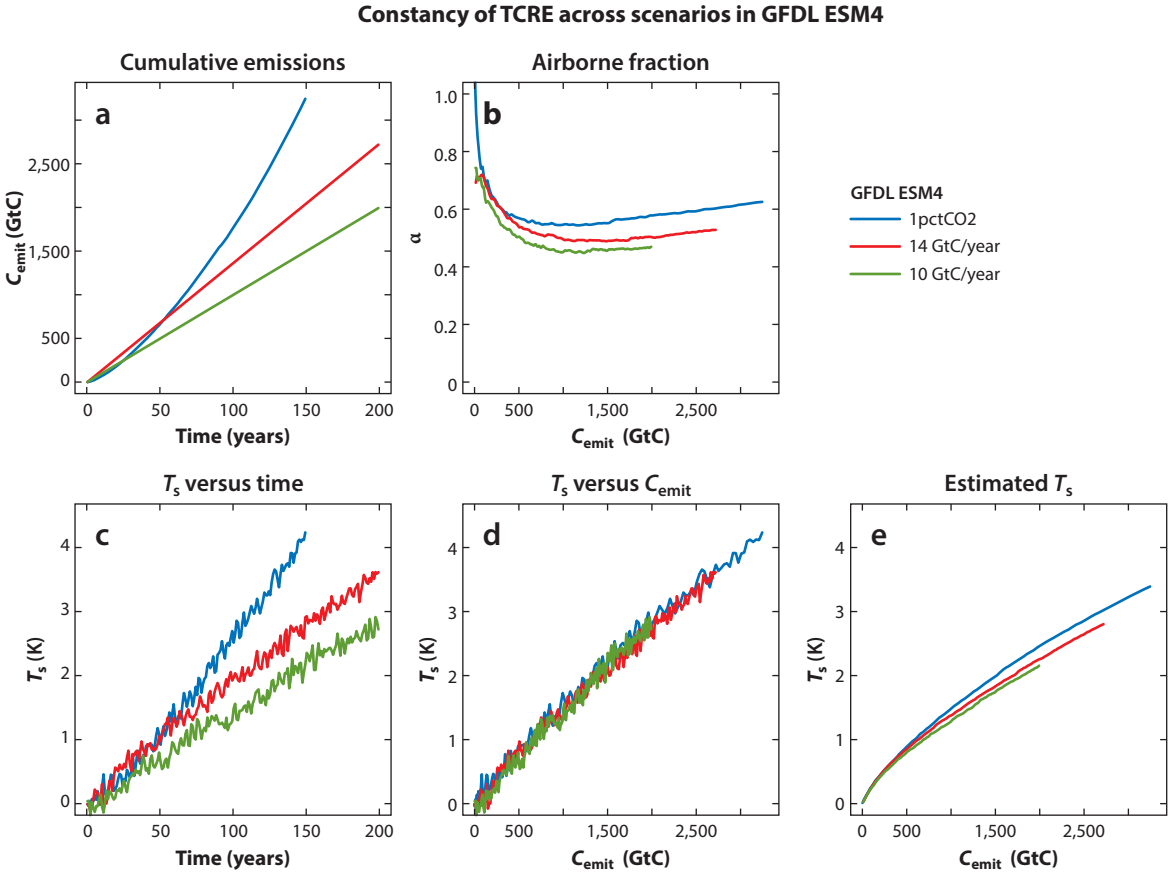


**Figure 6**

(*a*) Cumulative emissions $C_{\text{emit}}$ versus time for three scenarios (legend in *upper right*). (*b*) Airborne fraction $\alpha$ as a function of $C_{\text{emit}}$. (*c*) Temperature anomaly $T_s$ versus time. (*d*) $T_s$ versus $C_{\text{emit}}$. (*e*) $T_s$ as estimated from Equation 28. Temperature anomalies collapse when plotted as a function of $C_{\text{emit}}$ in panel *d*. This collapse is roughly reproduced by the estimated $T_s$ in panel *e*, thanks largely to airborne fractions that do not vary dramatically in time or across scenario (*panel b*).

(Equation 21), yielding

$$T_s \approx \frac{\ln\left(1+\alpha\frac{C_{\text{emit}}}{C_0}\right)}{\ln 2}\,\text{TCR} \qquad 28.$$

(Allen & Stocker 2014). This estimate is shown in **Figure 6*e***, computed using $\alpha(t)$ from **Figure 6*b***. The estimated $T_s$ curves (**Figure 6*e***) resemble the simulated ones (**Figure 6*d***) and also collapse onto a common curve (albeit with more spread). According to Equation 28, this rough collapse can be traced to the relative invariance of the airborne fraction $\alpha$ (**Figure 6*b***), which exhibits typical values of ~0.5 with variations of only ±10% or so across time or emissions scenarios.[16]

While Equation 28 is thus helpful in explaining the collapse of $T_s(C_{\text{emit}})$, the logarithmic dependence on $C_{\text{emit}}$ seems to contradict the linearity of $T_s$ with $C_{\text{emit}}$ (Equation 9). Indeed,

[16]Note also that the fractional spread in estimated $T_s(C_{\text{emit}})$ in **Figure 6*e*** is somewhat smaller than the fractional spread in airborne fraction in **Figure 6*b***, due to the logarithm in Equation 28.

concavity from the logarithm is clearly evident in **Figure 6*e***. Somehow, the logarithmic curvature in Equation 28 ends up being rectified in the simulated $T_s(C_{emit})$ in **Figure 6*d***. But we already saw in Equation 22 and **Figure 4** that deep ocean warming contributes to curvature between $\mathcal{F}$ and $T_s$, and this curvature ends up canceling the logarithmic curvature, yielding a fairly linear $T_s(C_{emit})$ (MacDougall & Friedlingstein 2015, MacDougall 2017).[17]

The constancy of TCRE across time and scenarios thus seems to result from a few fortuitous coincidences. This suggests that this constancy might fail under more extreme circumstances, such as widely varying emissions rates (Krasting et al. 2014) and/or strong carbon-climate feedbacks, such as permafrost carbon release (MacDougall & Friedlingstein 2015). The constancy of TCRE also seems to hinge critically on the behavior of the airborne fraction, which in ESM4 displays muted time and scenario dependence. These characteristics of $\alpha$ have been observed before (e.g., Gregory et al. 2009, Krasting et al. 2014, MacDougall & Friedlingstein 2015) but have been only sporadically studied (Raupach 2013, Seshadri 2017).

Finally, how does the explanation for the constancy of TCRE given above square with the discussion in Section 2.4, which derives a constant TCRE as a consequence of ZEC and linearity of the system? The same logic that led to Equation 28 can also be used to derive an analogous expression for the long-term ZEC shown in **Figure 1*b***, normalized by the temperature when emissions are zeroed out $T_{ze}$ (Tarshish et al. 2023):

$$\frac{\mathrm{ZEC}}{T_{ze}} = \frac{\ln\left(1 + \frac{\alpha_f C_{emit}}{C_0}\right)\mathrm{ECS}}{\ln\left(1 + \frac{\alpha_{ze} C_{emit}}{C_0}\right)\mathrm{TCR}} - 1. \qquad 29.$$

Here the airborne fraction again plays a key role, this time in the form of the final airborne fraction[18] $\alpha_f$ and the airborne fraction when emissions are zeroed $\alpha_{ze}$. Taylor-expanding for intuition yields

$$\frac{\mathrm{ZEC}}{T_{ze}} = \frac{\alpha_f/\alpha_{ze}}{\mathrm{TCR/ECS}} - 1. \qquad 30.$$

In this approximation (also recorded in **Table 1**), normalized ZEC results from the balance between chemical disequilibrium $\alpha_f/\alpha_{ze}$ when emissions are zeroed and the thermal disequilibrium TCR/ECS (Ehlert & Zickfeld 2017, Allen et al. 2022, Tarshish et al. 2023): If the chemical disequilibrium is greater ($\alpha_f/\alpha_{ze} < \mathrm{TCR/ECS}$), then $CO_2$ forcing will decline more than ocean heat uptake as the system equilibrates, leading to post-emissions cooling. Conversely, a greater thermal disequilibrium ($\mathrm{TCR/ECS} < \alpha_f/\alpha_{ze}$) will lead to post-emissions warming.

Evidently, ZEC $\approx 0$ results from these disequilibria taking on similar values. Similar to the constancy of TCRE, this seems not to be guaranteed but rather to result somewhat by chance [and indeed, some models do exhibit nonnegligible ZEC (Frölicher et al. 2014, MacDougall et al. 2020)]. Whether the coincidences behind ZEC $\approx 0$ and constant TCRE are the same or different remains to be clarified. The assumption of system linearity underlying Equation 11 also deserves scrutiny; relevant nonlinearities such as the logarithmic dependence of forcing on $CO_2$ concentration as well as carbon-climate feedbacks certainly exist, but whether they add up to sufficient nonlinearity to break the connection (Equation 11) between ZEC and constant TCRE is unclear.

[17] A related body of literature suggests that carbon-climate feedbacks associated with ocean carbon uptake also play a key role in this rectification (Goodwin et al. 2015, Williams et al. 2016), but how this relates to the behavior of the airborne fraction is at present unclear (MacDougall 2016).

[18] The final airborne fraction can be evaluated analytically using the buffered carbon inventory approximation of Goodwin et al. (2007), yielding estimates of around 0.2 (Tarshish et al. 2023). This estimate is in good agreement with carbon cycle models (e.g., Archer & Brovkin 2008).

## 7. OUTLOOK

We have now surveyed the climate sensitivity hierarchy of **Table 1** in some detail. In addition to reviewing progress in our understanding of forcing and feedback (Section 3), we have emphasized that:

- The TCR is broadly applicable to contemporary climate change via Equation 21, thanks to MLQE (Section 4).
- The shape of deep ocean heat uptake varies among models, in ways that the two-box model cannot account for (Section 5).
- ZEC and constant TCRE are equivalent in the limit of system linearity (Equation 11), but nonlinearities and apparent coincidences also play a role, complicating our understanding of these quantities (Section 6).

A heretofore undiscussed aspect of **Table 1** is the column of analytical expressions, which shows that each sensitivity measure encompasses the previous ones. The forcing and feedback from ECS are also part of the TCR; TCR is then itself part of TCRE. These sensitivity measures are thus all interconnected, and in particular, uncertainties in a given measure then propagate down to more complex measures. For example, uncertainties in TCR and ECS are relevant for uncertainty in ZEC (Jones & Friedlingstein 2020, Matthews et al. 2020).

Another aspect highlighted by this column is the introduction of additional key parameters as one increases complexity. Moving from ECS to TCR introduces the heat uptake coefficient $\gamma$; moving again from TCR to TCRE then introduces the airborne fraction $\alpha$. This simple observation suggests a path forward for our efforts: Just as much was learned through intense focus on $\mathcal{F}_{2\times}$ and $\lambda$, future progress may lie in a similar focus on $\gamma$ and $\alpha$. Despite the demonstrable relevance of TCR, TCRE, and ZEC for twenty-first-century climate change, there has been a relative dearth of research on understanding the heat uptake coefficient and airborne fraction. For instance, while we have analytical models that encapsulate some basic understanding of $\mathcal{F}_{2\times}$ and $\lambda$ (Equations 12 and 15) (see also Koll et al. 2023), no such understanding exists for $\gamma$. Recent work is beginning to generate new insight (e.g., Liu et al. 2023, Newsom et al. 2023, Gregory et al. 2024), but much more is needed to even out our understanding. This is all the more true for airborne fraction, where uncertainties in future land carbon uptake are notoriously large (Arora et al. 2020, Jones & Friedlingstein 2020) and theoretical efforts have been few (Raupach 2013, Seshadri 2017).

As for ECS, given the complications of studying ECS in AOGCMs (Section 2.2), it may be worth returning to the practice of simulating ECS with SOMs. Admittedly, the assumption of fixed ocean heat flux convergence can be an unnatural one, particularly in regions of sea-ice retreat. But from a global mean point of view focused on climate sensitivity, SOMs provide a convenient method for assessing changes in ECS due to incremental model development (Gettelman et al. 2012, 2019) and are no less accurate at estimating ECS than extrapolation methods (Dunne et al. 2020b). Indeed, it may even be appropriate to reconsider ECS as primarily a property of SOMs, useful as a modeling benchmark and an overall measure of global warming, rather than as a fundamental property of the Earth system that climate science must accurately pin down (see discussion in Knutti & Rugenstein 2015, Dunne et al. 2020b, Meehl et al. 2020).

Finally, it is interesting to note that while TCR has a precise definition as the warming around year 70 of 1pctCO2 simulations, and ECS has a precise definition (at least in principle) as equilibrium warming due to a doubling of $CO_2$, the same is not true for TCRE and ZEC. Standard scenarios for calculating them have not been agreed upon, nor has the timescale over which ZEC is assessed, so at present it is not possible to speak of *the* TCRE or ZEC for a given model.

The holistic view of climate sensitivity here presents a gauntlet for climate science; it has been challenging enough to narrow the error bars on purely atmospheric forcing and feedback, let alone

add in interactions with the ocean and carbon cycle. But for climate sensitivity to be relevant as we project the future and assess the feasibility of our climate targets, such a holistic understanding seems to be required.

## DISCLOSURE STATEMENT

The authors are not aware of any affiliations, memberships, funding, or financial holdings that might be perceived as affecting the objectivity of this review.

## ACKNOWLEDGMENTS

We acknowledge useful feedback from Isaac Held, Mike Winton, Andrew Williams, Tristan Abbott, Nathaniel Tarshish, and Laure Zanna.

## LITERATURE CITED

Allen MR, Frame DJ, Huntingford C, Jones CD, Lowe JA, et al. 2009. Warming caused by cumulative carbon emissions towards the trillionth tonne. *Nature* 458(7242):1163–66

Allen MR, Friedlingstein P, Girardin CA, Jenkins S, Malhi Y, et al. 2022. Net zero: science, origins, and implications. *Annu. Rev. Environ. Resourc.* 47:849–87

Allen MR, Stocker TF. 2014. Impact of delay in reducing carbon dioxide emissions. *Nat. Clim. Change* 4(1):23–26

Andrews T, Bodas-Salcedo A, Gregory JM, Dong Y, Armour KC, et al. 2022. On the effect of historical SST patterns on radiative feedback. *J. Geophys. Res. Atmos.* 127(18):e2022JD036675

Andrews T, Gregory JM, Forster PM, Webb MJ. 2012a. Cloud adjustment and its role in $CO_2$ radiative forcing and climate sensitivity: a review. *Surv. Geophys.* 33:619–35

Andrews T, Gregory JM, Webb MJ. 2015. The dependence of radiative forcing and feedback on evolving patterns of surface temperature change in climate models. *J. Clim.* 28(4):1630–48

Andrews T, Gregory JM, Webb MJ, Taylor KE. 2012b. Forcing, feedbacks and climate sensitivity in CMIP5 coupled atmosphere-ocean climate models. *Geophys. Res. Lett.* 39(9):L09712

Archer D, Brovkin V. 2008. The millennial atmospheric lifetime of anthropogenic $CO_2$. *Clim. Change* 90(3):283–97

Armour KC, Bitz CM, Roe GH. 2013. Time-varying climate sensitivity from regional feedbacks. *J. Clim.* 26(13):4518–34

Armour KC, Proistosescu C, Dong Y, Hahn LC, Blanchard-Wrigglesworth E, et al. 2024. Sea-surface temperature pattern effects have slowed global warming and biased warming-based constraints on climate sensitivity. *PNAS* 121(12):e2312093121

Arora VK, Katavouta A, Williams RG, Jones CD, Brovkin V, et al. 2020. Carbon-concentration and carbon-climate feedbacks in CMIP6 models and their comparison to CMIP5 models. *Biogeosciences* 17(16):4173–222

Arrhenius S. 1896. On the influence of carbonic acid in the air upon the temperature of the ground. *Philos. Mag. J. Sci.* 41:237–76

Bellouin N, Quaas J, Gryspeerdt E, Kinne S, Stier P, et al. 2020. Bounding global aerosol radiative forcing of climate change. *Rev. Geophys.* 58(1):e2019RG000660

Caldwell PM, Zelinka MD, Taylor KE, Marvel K. 2016. Quantifying the sources of intermodel spread in equilibrium climate sensitivity. *J. Clim.* 29(2):513–24

Callendar GS. 1938. The artificial production of carbon dioxide and its influence on temperature. *Q. J. R. Meteorol. Soc.* 64(275):223–40

Canadell J, Monteiro P, Costa M, da Cunha LC, Cox P, et al. 2021. Global carbon and other biogeochemical cycles and feedbacks. In *Climate Change 2021: The Physical Science Basis. Contribution of Working Group I to the Sixth Assessment Report of the Intergovernmental Panel on Climate Change Basis*, ed. V Masson-Delmotte, P Zhai, A Pirani, SL Connors, C Péan et al., pp. 673–816. Cambridge, UK: Cambridge Univ. Press

Ceppi P, Brient F, Zelinka MD, Hartmann DL. 2017. Cloud feedback mechanisms and their representation in global climate models. *Wiley Interdiscip. Rev. Clim. Change* 8(4):e465

Ceppi P, Gregory JM. 2017. Relationship of tropospheric stability to climate sensitivity and Earth's observed radiation budget. *PNAS* 114(50):13126–31

Ceppi P, Nowack P. 2021. Observational evidence that cloud feedback amplifies global warming. *PNAS* 118(30):e2026290118

Cess RD, Potter GL, Blanchet JP, Boer GJ, Ghan SJ, et al. 1989. Interpretation of cloud-climate feedback as produced by 14 atmospheric general circulation models. *Science* 245(4917):513–16

Charney J, Arakawa A, Baker DJ, Bolin B, Dickinson RE, et al. 1979. *Carbon dioxide and climate: a scientific assessment*. Tech. rep., Natl. Acad. Sci., Washington, DC

Colman R, Soden BJ. 2021. Water vapor and lapse rate feedbacks in the climate system. *Rev. Mod. Phys.* 93(4):045002

Cowtan K, Hausfather Z, Hawkins E, Jacobs P, Mann ME, et al. 2015. Robust comparison of climate models with observations using blended land air and ocean sea surface temperatures. *Geophys. Res. Lett.* 42(15):6526–34

Cronin TW, Dutta I. 2023. How well do we understand the Planck feedback? *J. Adv. Model. Earth Syst.* 15(7):e2023MS003729

Danabasoglu G, Gent PR. 2009. Equilibrium climate sensitivity: Is it accurate to use a slab ocean model? *J. Clim.* 22(9):2494–99

Donner LJ, Wyman BL, Hemler RS, Horowitz LW, Ming Y, et al. 2011. The dynamical core, physical parameterizations, and basic simulation characteristics of the atmospheric component AM3 of the GFDL global coupled model CM3. *J. Clim.* 24(13):3484–519

Dunne JP, Horowitz LW, Adcroft AJ, Ginoux P, Held IM, et al. 2020a. The GFDL Earth System Model version 4.1 (GFDL-ESM 4.1): overall coupled model description and simulation characteristics. *J. Adv. Model. Earth Syst.* 12(11):e2019MS002015

Dunne JP, Winton M, Bacmeister J, Danabasoglu G, Gettelman A, et al. 2020b. Comparison of equilibrium climate sensitivity estimates from slab ocean, 150-year, and longer simulations. *Geophys. Res. Lett.* 47(16):e2020GL088852

Ehlert D, Zickfeld K. 2017. What determines the warming commitment after take back cessation of $CO_2$ emissions? *Environ. Res. Lett.* 12(1):015002

Eyring V, Bony S, Meehl GA, Senior CA, Stevens B, et al. 2016. Overview of the Coupled Model Intercomparison Project Phase 6 (CMIP6) experimental design and organization. *Geosci. Model Dev.* 9(5):1937–58

Feng J, Paynter D, Menzel R. 2023. How a stable greenhouse effect on Earth is maintained under global warming. *J. Geophys. Res. Atmos.* 128(9):e2022JD038124

Forster PM. 2016. Inference of climate sensitivity from analysis of Earth's energy budget. *Annu. Rev. Earth Planet. Sci.* 44:85–106

Forster PM, Storelvmo T, Armour KC, Collins W, Dufresne JL, et al. 2021. The Earth's energy budget, climate feedbacks, and climate sensitivity. In *Climate Change 2021: The Physical Science Basis. Contribution of Working Group I to the Sixth Assessment Report of the Intergovernmental Panel on Climate Change*, ed. V Masson-Delmotte, P Zhai, A Pirani, SL Connors, C Péan et al., pp. 923–1054. Cambridge, UK: Cambridge Univ. Press

Friedlingstein P, O'Sullivan M, Jones MW, Andrew RM, Hauck J, et al. 2020. Global carbon budget 2020. *Earth Syst. Sci. Data* 12(4):3269–340

Frölicher TL, Winton M, Sarmiento JL. 2014. Continued global warming after $CO_2$ emissions stoppage. *Nat. Clim. Change* 4(1):40–44

Geoffroy O, Saint-Martin D, Bellon G, Voldoire A, Olivié DJ, Tytéca S. 2013a. Transient climate response in a two-layer energy-balance model. Part II: Representation of the efficacy of deep-ocean heat uptake and validation for CMIP5 AOGCMs. *J. Clim.* 26(6):1859–76

Geoffroy O, Saint-Martin D, Olivié DJ, Voldoire A, Bellon G, Tytéca S. 2013b. Transient climate response in a two-layer energy-balance model. Part I: Analytical solution and parameter calibration using CMIP5 AOGCM experiments. *J. Clim.* 26(6):1841–57

Gettelman A, Hannay C, Bacmeister JT, Neale RB, Pendergrass AG, et al. 2019. High climate sensitivity in the Community Earth System Model Version 2 (CESM2). *Geophys. Res. Lett.* 46(14):8329–37

Gettelman A, Kay JE, Shell KM. 2012. The evolution of climate sensitivity and climate feedbacks in the community atmosphere model. *J. Clim.* 25(5):1453–69

Gillett NP, Arora VK, Matthews D, Allen MR. 2013. Constraining the ratio of global warming to cumulative $CO_2$ emissions using CMIP5 simulations. *J. Clim.* 26(18):6844–58

Gillett NP, Arora VK, Zickfeld K, Marshall SJ, Merryfield WJ. 2011. Ongoing climate change following a complete cessation of carbon dioxide emissions. *Nat. Geosci.* 4(2):83–87

Goodwin P, Williams RG, Follows MJ, Dutkiewicz S. 2007. Ocean-atmosphere partitioning of anthropogenic carbon dioxide on centennial timescales. *Glob. Biogeochem. Cycles* 21(1):GB1014

Goodwin P, Williams RG, Ridgwell A. 2015. Sensitivity of climate to cumulative carbon emissions due to compensation of ocean heat and carbon uptake. *Nat. Geosci.* 8(1):29–34

Gregory JM, Andrews T. 2016. Variation in climate sensitivity and feedback parameters during the historical period. *Geophys. Res. Lett.* 43(8):3911–20

Gregory JM, Andrews T, Good P. 2015. The inconstancy of the transient climate response parameter under increasing $CO_2$. *Philos. Trans. R. Soc. A* 373(2054):20140417

Gregory JM, Bloch-Johnson J, Couldrey MP, Exarchou E, Griffies SM, et al. 2024. A new conceptual model of global ocean heat uptake. *Clim. Dyn.* 62(3):1669–713

Gregory JM, Forster PM. 2008. Transient climate response estimated from radiative forcing and observed temperature change. *J. Geophys. Res.* 113(D23):D23105

Gregory JM, Ingram WJ, Palmer MA, Jones GS, Stott PA, et al. 2004. A new method for diagnosing radiative forcing and climate sensitivity. *Geophys. Res. Lett.* 31(3):2–5

Gregory JM, Jones CD, Cadule P, Friedlingstein P. 2009. Quantifying carbon cycle feedbacks. *J. Clim.* 22(19):5232–50

Grose MR, Gregory J, Colman R, Andrews T. 2018. What climate sensitivity index is most useful for projections? *Geophys. Res. Lett.* 45(3):1559–66

Hansen J, Lacis AA, Rind DH, Russell GL, Stone P, et al. 1984. Climate sensitivity: analysis of feedback mechanisms. *Clim. Process. Clim. Sensit.* 29:130–63

Hansen J, Sato M, Ruedy R. 1997. Radiative forcing and climate response. *J. Geophys. Res.* 102(D6):6831–64

Hansen J, Sato M, Ruedy R, Nazarenko L, Lacis A, et al. 2005. Efficacy of climate forcings. *J. Geophys. Res.* 110(D18):D18104

Hartmann DL, Larson K. 2002. An important constraint on tropical cloud - climate feedback. *Geophys. Res. Lett.* 29(20):1951

Harvey LDD. 2018. *Global Warming: The Hard Science*. Boca Raton, FL: Routledge

He H, Kramer RJ, Soden BJ, Jeevanjee N. 2023. State dependence of $CO_2$ forcing and its implications for climate sensitivity. *Science* 382(6674):1051–56

Held IM, Guo H, Adcroft A, Dunne JP, Horowitz LW, et al. 2019. Structure and performance of GFDL's CM4.0 climate model. *J. Adv. Model. Earth Syst.* 11(11):3691–727

Held IM, Shell KM. 2012. Using relative humidity as a state variable in climate feedback analysis. *J. Clim.* 25(8):2578–82

Held IM, Winton M, Takahashi K, Delworth T, Zeng F, Vallis GK. 2010. Probing the fast and slow components of global warming by returning abruptly to preindustrial forcing. *J. Clim.* 23(9):2418–27

Herrington T, Zickfeld K. 2014. Path independence of climate and carbon cycle response over a broad range of cumulative carbon emissions. *Earth Syst. Dyn.* 5(2):409–22

Hoffert MI, Callegari AJ, Hsieh CT. 1980. The role of deep sea heat storage in the secular response to climatic forcing. *J. Geophys. Res.* 85(C11):6667–79

Houghton JT, Meira Filho L, Bruce J, Lee H, Callander B, et al., eds. 1994. *Climate Change 1994: Radiative Forcing of Climate Change and an Evaluation of the IPCC 1992 IS92 Emission Scenarios.* Cambridge, UK: Cambridge Univ. Press

Hulburt EO. 1931. The temperature of the lower atmosphere of the Earth. *Phys. Rev.* 38(10):1876–90

Ingram WJ. 2010. A very simple model for the water vapour feedback on climate change. *Q. J. R. Meteorol. Soc.* 136(646):30–40

Ingram WJ. 2013. A new way of quantifying GCM water vapour feedback. *Clim. Dyn.* 40(3–4):913–24
Jeevanjee N. 2023. Climate sensitivity from radiative-convective equilibrium: a chalkboard approach. *Am. J. Phys.* 91(9):731–45
Jeevanjee N, Held I, Ramaswamy V. 2022. Manabe's radiative-convective equilibrium. *Bull. Am. Meteorol. Soc.* 103(11):E2533–43
Jeevanjee N, Koll DDB, Lutsko NJ. 2021a. "Simpson's Law" and the spectral cancellation of climate feedbacks. *Geophys. Res. Lett.* 48(14):e2021GL093699
Jeevanjee N, Seeley JT, Paynter D, Fueglistaler S. 2021b. An analytical model for spatially varying clear-sky $CO_2$ forcing. *J. Clim.* 34(23):9463–80
Jones CD, Friedlingstein P. 2020. Quantifying process-level uncertainty contributions to TCRE and carbon budgets for meeting Paris Agreement climate targets. *Environ. Res. Lett.* 15(7):074019
Kamae Y, Watanabe M, Ogura T, Yoshimori M, Shiogama H. 2015. Rapid adjustments of cloud and hydrological cycle to increasing $CO_2$: a review. *Curr. Clim. Change Rep.* 1:103–13
Klein SA, Hall A, Norris JR, Pincus R. 2017. Low-cloud feedbacks from cloud-controlling factors: a review. *Surv. Geophys.* 38(6):1307–29
Knutti R, Hegerl GC. 2008. The equilibrium sensitivity of the Earth's temperature to radiation changes. *Nat. Geosci.* 1:735–43
Knutti R, Rugenstein M. 2015. Feedbacks, climate sensitivity and the limits of linear models. *Philos. Trans. R. Soc. A* 373(2054):20150146
Koll DDB, Cronin TW. 2018. Earth's outgoing longwave radiation linear due to $H_2O$ greenhouse effect. *PNAS* 115(41):10293–98
Koll DDB, Jeevanjee N, Lutsko NJ. 2023. An analytic model for the clear-sky longwave feedback. *J. Atmos. Sci.* 80(8):1923–51
Krasting JP, Dunne JP, Shevliakova E, Stouffer RJ. 2014. Trajectory sensitivity of the transient climate response to cumulative carbon emissions. *Geophys. Res. Lett.* 41:2520–27
Krasting JP, Stouffer RJ, Griffies SM, Hallberg RW, Malyshev SL, et al. 2018. Role of ocean model formulation in climate response uncertainty. *J. Clim.* 31(22):9313–33
Kuhlbrodt T, Gregory JM. 2012. Ocean heat uptake and its consequences for the magnitude of sea level rise and climate change. *Geophys. Res. Lett.* 39(17):L18608
Lee S, L'Heureux M, Wittenberg AT, Seager R, O'Gorman PA, Johnson NC. 2022. On the future zonal contrasts of equatorial Pacific climate: perspectives from observations, simulations, and theories. *NPJ Clim. Atmos. Sci.* 5:82
Li C, von Storch JS, Marotzke J. 2013. Deep-ocean heat uptake and equilibrium climate response. *Clim. Dyn.* 40(5–6):1071–86
Liu M, Soden BJ, Vecchi GA, Wang C. 2023. The spread of ocean heat uptake efficiency traced to ocean salinity. *Geophys. Res. Lett.* 50(4):e2022GL100171
Lunt DJ, Haywood AM, Schmidt GA, Salzmann U, Valdes PJ, Dowsett HJ. 2010. Earth system sensitivity inferred from Pliocene modelling and data. *Nat. Geosci.* 3(1):60–64
MacDougall AH. 2016. The transient response to cumulative $CO_2$ emissions: a review. *Curr. Clim. Change Rep.* 2(1):39–47
MacDougall AH. 2017. The oceanic origin of path-independent carbon budgets. *Sci. Rep.* 7(1):10373
MacDougall AH, Friedlingstein P. 2015. The origin and limits of the near proportionality between climate warming and cumulative $CO_2$ emissions. *J. Clim.* 28(10):4217–30
MacDougall AH, Frölicher TL, Jones CD, Rogelj J, Matthews HD, et al. 2020. Is there warming in the pipeline? A multi-model analysis of the Zero Emissions Commitment from $CO_2$. *Biogeosciences* 17(11):2987–3016
Manabe S, Stouffer RJ. 1980. Sensitivity of a global climate model to an increase of $CO_2$ concentration in the atmosphere. *J. Geophys. Res.* 85(C10):5529–54
Manabe S, Stouffer RJ, Spelman MJ, Bryan K. 1991. Transient responses of a coupled ocean–atmosphere model to gradual changes of atmospheric $CO_2$. Part I. Annual mean response. *J. Clim.* 4(8):785–818
Manabe S, Wetherald RT. 1967. Thermal equilibrium of the atmosphere with a given distribution of relative humidity. *J. Atmos. Sci.* 24(3):241–59

Manabe S, Wetherald RT. 1975. The effects of doubling the $CO_2$ concentration on the climate of a general circulation model. *J. Atmos. Sci.* 32(1):3–15
Marshall DP, Zanna L. 2014. A conceptual model of ocean heat uptake under climate change. *J. Clim.* 27(22):8444–65
Matthews HD, Caldeira K. 2008. Stabilizing climate requires near-zero emissions. *Geophys. Res. Lett.* 35(4):L04705
Matthews HD, Gillett NP, Stott PA, Zickfeld K. 2009. The proportionality of global warming to cumulative carbon emissions. *Nature* 459(7248):829–32
Matthews HD, Solomon S, Pierrehumbert RT. 2012. Cumulative carbon as a policy framework for achieving climate stabilization. *Philos. Trans. R. Soc. A* 370(1974):4365–79
Matthews HD, Tokarska KB, Nicholls ZR, Rogelj J, Canadell JG, et al. 2020. Opportunities and challenges in using remaining carbon budgets to guide climate policy. *Nat. Geosci.* 13(12):769–79
McFarlane NA, Boer GJ, Blanchet JP, Lazare M. 1992. The Canadian Climate Centre second-generation general circulation model and its equilibrium climate. *J. Clim.* 5(10):1013–44
McKim B, Bony S, Dufresne JL. 2024. Weak anvil cloud area feedback suggested by physical and observational constraints. *Nat. Geosci.* 17(5):392–97
Meehl GA, Covey C, McAvaney B, Latif M, Stouffer RJ. 2005. Overview of the Coupled Model Intercomparison Project. *Bull. Am. Meteorol. Soc.* 86(1):89–93
Meehl GA, Senior CA, Eyring V, Flato G, Lamarque JF, et al. 2020. Context for interpreting equilibrium climate sensitivity and transient climate response from the CMIP6 Earth system models. *Sci. Adv.* 6(26):eaba1981
Mitchell J, Manabe S, Meleshko V, Tokioka T. 1990. Equilibrium climate change and its implications for the future. In *Climate Change: The IPCC Scientific Assessment*, ed. JT Houghton, GJ Jenkins, JJ Ephraums, pp. 131–72. Cambridge, UK: Cambridge Univ. Press
Myers TA, Scott RC, Zelinka MD, Klein SA, Norris JR, Caldwell PM. 2021. Observational constraints on low cloud feedback reduce uncertainty of climate sensitivity. *Nat. Clim. Change* 11(6):501–7
Myhre G, Byrom RE, Andrews T, Forster PM, Smith CJ. 2024. Efficacy of climate forcings in transient CMIP6 simulations. *Front. Clim.* 6(1):1397358
Newsom E, Zanna L, Gregory J. 2023. Background pycnocline depth constrains future ocean heat uptake efficiency. *Geophys. Res. Lett.* 50:e2023GL105673
Nijsse F, Cox P, Williamson M. 2020. An emergent constraint on transient climate response from simulated historical warming in CMIP6 models. *Earth Syst. Dyn.* 11(3):737–50
O'Neill BC, Tebaldi C, Van Vuuren DP, Eyring V, Friedlingstein P, et al. 2016. The Scenario Model Intercomparison Project (ScenarioMIP) for CMIP6. *Geosci. Model Dev.* 9(9):3461–82
Otto A, Otto FE, Boucher O, Church J, Hegerl G, et al. 2013. Energy budget constraints on climate response. *Nat. Geosci.* 6(6):415–16
Palazzo Corner S, Siegert M, Ceppi P, Fox-Kemper B, Frölicher TL, et al. 2023. The Zero Emissions Commitment and climate stabilization. *Front. Sci.* 1:1170744
Paynter D, Frölicher TL, Horowitz LW, Silvers LG. 2018. Equilibrium climate sensitivity obtained from multimillennial runs of two GFDL climate models. *J. Geophys. Res. Atmos.* 123(4):1921–41
Plass GN. 1956. The influence of the 15$\mu$ carbon-dioxide band on the atmospheric infra-red cooling rate. *Q. J. R. Meteorol. Soc.* 82(353):310–24
Previdi M, Liepert BG, Peteet D, Hansen J, Beerling DJ, et al. 2013. Climate sensitivity in the Anthropocene. *Q. J. R. Meteorol. Soc.* 139(674):1121–31
Ramaswamy V, Collins W, Haywood J, Lean J, Mahowald N, et al. 2019. Radiative forcing of climate: the historical evolution of the radiative forcing concept, the forcing agents and their quantification, and applications. *Meteorol. Monogr.* 59:14.1–.101
Randall DA, Wood R, Bony S, Colman R, Fichefet T, et al. 2007. Climate models and their evaluation. In *Climate Change 2007: The Physical Science Basis. Contribution of Working Group I to the Fourth Assessment Report of the Intergovernmental Panel on Climate Change*, ed. S Solomon, D Qin, M Manning, M Marquis, K Averyt, et al., pp. 589–662. Cambridge, UK: Cambridge Univ. Press
Raper SC, Gregory JM, Stouffer RJ. 2002. The role of climate sensitivity and ocean heat uptake on AOGCM transient temperature response. *J. Clim.* 15(3):124–30

Raupach MR. 2013. The exponential eigenmodes of the carbon-climate system, and their implications for ratios of responses to forcings. *Earth Syst. Dyn.* 4(1):31–49

Richardson TB, Forster PM, Smith CJ, Maycock AC, Wood T, et al. 2019. Efficacy of climate forcings in PDRMIP models. *J. Geophys. Res. Atmos.* 124(23):12824–44

Roe G. 2009. Feedbacks, timescales, and seeing red. *Annu. Rev. Earth Planet. Sci.* 37:93–115

Roemer FE, Buehler SA, Brath M, Kluft L, John VO. 2023. Direct observation of Earth's spectral long-wave feedback parameter. *Nat. Geosci.* 16(5):416–21

Rogelj J, Forster PM, Kriegler E, Smith CJ, Séférian R. 2019. Estimating and tracking the remaining carbon budget for stringent climate targets. *Nature* 571(7765):335–42

Romps DM, Seeley JT, Edman JP. 2022. Why the forcing from carbon dioxide scales as the logarithm of its concentration. *J. Clim.* 35(13):4027–47

Rose BEJ, Rayborn L. 2016. The effects of ocean heat uptake on transient climate sensitivity. *Curr. Clim. Change Rep.* 2:190–201

Rugenstein M, Armour KC. 2021. Three flavors of radiative feedbacks and their implications for estimating equilibrium climate sensitivity. *Geophys. Res. Lett.* 48(15):e2021GL092983

Rugenstein M, Bloch-Johnson J, Gregory J, Andrews T, Mauritsen T, et al. 2020. Equilibrium climate sensitivity estimated by equilibrating climate models. *Geophys. Res. Lett.* 47(4):e2019GL083898

Rugenstein M, Zelinka M, Karnauskas K, Ceppi P, Andrews T. 2023. Patterns of surface warming matter for climate sensitivity. *Eos* 104. **https://doi.org/10.1029/2023EO230411**

Seeley JT. 2018. *Convection, radiation, and climate: fundamental mechanisms and impacts of a changing atmosphere*. PhD thesis, Univ. Calif., Berkeley

Seneviratne SI, Donat MG, Pitman AJ, Knutti R, Wilby RL. 2016. Allowable $CO_2$ emissions based on regional and impact-related climate targets. *Nature* 529(7587):477–83

Seshadri AK. 2017. Origin of path independence between cumulative $CO_2$ emissions and global warming. *Clim. Dyn.* 49(9–10):3383–401

Sherwood SC, Bony S, Boucher O, Bretherton CS, Forster PM, et al. 2015. Adjustments in the forcing-feedback framework for understanding climate change. *Bull. Am. Meteorol. Soc.* 96(2):217–28

Sherwood SC, Webb MJ, Annan JD, Armour KC, Forster PM, et al. 2020. An assessment of Earth's climate sensitivity using multiple lines of evidence. *Rev. Geophys.* 58(4):e2019RG000678

Siebesma AP, Bony S, Jakob C, Stevens B, eds. 2020. *Clouds and Climate: Climate Science's Greatest Challenge*. Cambridge, UK: Cambridge Univ. Press

Smith CJ, Kramer RJ, Myhre G, Alterskjr K, Collins W, et al. 2020. Effective radiative forcing and adjustments in CMIP6 models. *Atmos. Chem. Phys.* 20(16):9591–618

Soden BJ, Broccoli AJ, Hemler RS. 2004. On the use of cloud forcing to estimate cloud feedback. *J. Clim.* 17(19):3661–65

Solomon S, Plattner GK, Knutti R, Friedlingstein P. 2009. Irreversible climate change due to carbon dioxide emissions. *PNAS* 106(6):1704–9

Stevens B, Kluft L. 2023. A colorful look at climate sensitivity. *Atmos. Chem. Phys.* 23:14673–89

Stevens B, Sherwood SC, Bony S, Webb MJ. 2016. Prospects for narrowing bounds on Earth's equilibrium climate sensitivity. *Earth's Future* 4(11):512–22

Stouffer RJ, Manabe S. 1999. Response of a coupled ocean-atmosphere model to increasing atmospheric carbon dioxide: sensitivity to the rate of increase. *J. Clim.* 12(8):2224–37

Stouffer RJ, Manabe S. 2017. Assessing temperature pattern projections made in 1989. *Nat. Clim. Change* 7(3):163–65

Sutton RT, Dong B, Gregory JM. 2007. Land/sea warming ratio in response to climate change: IPCC AR4 model results and comparison with observations. *Geophys. Res. Lett.* 34(2):2–6

Szopa S, Naik V, Adhikary B, Artaxo P, Berntsen T, et al. 2021. Short-lived climate forcers. In *Climate Change 2021: The Physical Science Basis. Contribution of Working Group I to the Sixth Assessment Report of the Intergovernmental Panel on Climate Change*, ed. V Masson-Delmotte, P Zhai, A Pirani, SL Connors, C Péan et al., pp. 817–921. Cambridge, UK: Cambridge Univ. Press

Tarshish N, Jeevanjee N, Fung I. 2023. Emissions cessation yields multi-century cooling. *Res. Square*. **https://doi.org/10.21203/rs.3.rs-3607244/v1**

Taylor KE, Stouffer RJ, Meehl GA. 2012. An overview of CMIP5 and the experiment design. *Bull. Am. Meteorol. Soc.* 93(4):485–98

Thompson DWJ, Bony S, Li Y. 2017. Thermodynamic constraint on the depth of the global tropospheric circulation. *PNAS* 114(31):8181–86

Washington WM, Meehl GA. 1989. Climate sensitivity due to increased $CO_2$: experiments with a coupled atmosphere and ocean general circulation model. *Clim. Dyn.* 4(1):1–38

Watanabe M, Kang SM, Collins M, Hwang YT, McGregor S, Stuecker MF. 2024. Possible shift in controls of the tropical Pacific surface warming pattern. *Nature* 630:315–24

Wigley TML, Schlesinger ME. 1985. Analytical solution for the effect of increasing $CO_2$ on global mean temperature. *Nature* 315(6021):649–52

Williams RG, Goodwin P, Roussenov VM, Bopp L. 2016. A framework to understand the transient climate response to emissions. *Environ. Res. Lett.* 11(1):015003

Wills RC, Dong Y, Proistosecu C, Armour KC, Battisti DS. 2022. Systematic climate model biases in the large-scale patterns of recent sea-surface temperature and sea-level pressure change. *Geophys. Res. Lett.* 49(17):e2022GL100011

Wilson DJ, Gea-Banacloche J. 2012. Simple model to estimate the contribution of atmospheric $CO_2$ to the Earth's greenhouse effect. *Am. J. Phys.* 80(4):306–15

Winton M, Adcroft A, Dunne JP, Held IM, Shevliakova E, et al. 2020. Climate sensitivity of GFDL's CM4.0. *J. Adv. Model. Earth Syst.* 12(1):e2019MS001838

Winton M, Takahashi K, Held IM. 2010. Importance of ocean heat uptake efficacy to transient climate change. *J. Clim.* 23(9):2333–44

Wordsworth RD, Seeley JT, Shine KP. 2024. Fermi resonance and the quantum mechanical basis of global warming. *Planet. Sci. J.* 5(3):67

Yoshimori M, Lambert FH, Webb MJ, Andrews T. 2020. Fixed anvil temperature feedback: positive, zero, or negative? *J. Clim.* 33(7):2719–39

Zelinka MD, Randall DA, Webb MJ, Klein SA. 2017. Clearing clouds of uncertainty. *Nat. Clim. Change* 7(10):674–78

Zhang Y, Jeevanjee N, Fueglistaler S. 2020. Linearity of outgoing longwave radiation: from an atmospheric column to global climate models. *Geophys. Res. Lett.* 47(17):e2020GL089235

Zhao M, Golaz JC, Held IM, Guo H, Balaji V, et al. 2018. The GFDL Global Atmosphere and Land Model AM4.0/LM4.0: 2. Model description, sensitivity studies, and tuning strategies. *J. Adv. Model. Earth Syst.* 10(3):735–69